INTERNATIONAL JOURNAL OF
NUMERICAL ANALYSIS AND MODELING
Volume 21, Number 4, Pages 528–559

doi: 10.4208/ijnam2024-1021

hp-VERSION ANALYSIS FOR ARBITRARILY SHAPED ELEMENTS ON THE BOUNDARY DISCONTINUOUS GALERKIN METHOD FOR STOKES SYSTEMS

EFTHYMIOS N. KARATZAS

Abstract. In the present work, we examine and analyze an *hp*-version interior penalty discontinuous Galerkin finite element method for the numerical approximation of a steady fluid system on computational meshes consisting of polytopic elements on the boundary. This approach is based on the discontinuous Galerkin method, enriched by arbitrarily shaped elements techniques as has been introduced in [13]. In this framework, and employing extensions of trace, Markov-type, and H^1/L^2-type inverse estimates to arbitrary element shapes, we examine a stationary Stokes fluid system enabling the proof of the inf/sup condition and the *hp*- a priori error estimates, while we investigate the optimal convergence rates numerically. This approach recovers and integrates the flexibility and superiority of the discontinuous Galerkin methods for fluids whenever geometrical deformations are taking place by degenerating the edges, facets, of the polytopic elements only on the boundary, combined with the efficiency of the *hp*-version techniques based on arbitrarily shaped elements without requiring any mapping from a given reference frame.

Key words. Arbitrarily shaped elements, discontinuous Galerkin finite element method, hp-version stability, a-priori error estimates, fluid dynamics.

1. Introduction

Recent years have shown scientists' interest significantly focused on the context of Galerkin finite element methods. This effort has given birth to new methods based on general-shaped elements which arise computational complexity reduction, like mimetic finite difference methods [9], virtual element methods [8], various discontinuous Galerkin approaches such as interior penalty Galerkin methods [14], and hybridized discontinuous Galerkin [15, 18], which are very attractive and used by the engineering and mathematics community. We continue by reporting more works related to discontinuous Galerkin (dG) methods, similar finite element frameworks, and advances, *h*- or *hp*- version, fluid and Stokes systems related literature. We also introduce the skeleton of the present work. Hence, other approaches have involved non-polynomial approximation spaces like polygonal and other generalized finite element methods, [26, 54]. We refer to [14] for admissible polygonal/polyhedral element shapes for which the general interior penalty discontinuous Galerkin method (IP-dG), appears both stable and convergent while generalizes under mild assumptions the validity of standard approximation results, such as inverse estimates, best approximation estimates, and extension theorems.

In a *p*-version Galerkin framework achieving exponential convergence, for smooth partial differential equation problems defined on generally curved domains using isoparametrically mapped elements, we recall [46, 47], while for non-linear maps on element patches that are used to represent domain geometry we refer to [45, 53]. Although in both cases, as the polynomial order increases, the aforementioned mapping appears very costly and/or difficult to construct and implement in practice.

Received by the editors on September 7, 2023 and, accepted on April 30, 2024.
2000 *Mathematics Subject Classification.* 35Q35, 76M10, 35Q30.

For Stokes flow systems, in [4, 55], an *hp*-discontinuous Galerkin approximation that shows better stability properties than the corresponding conforming ones is examined with finite element triangulation not required to be conforming employing discontinuous pressures and velocities, while it is defined on the interfaces between the elements involving the jumps of the velocity and the average of the pressure. The work of [28] also, describes a family of dG finite element methods formulated and analyzed for Stokes and Navier-Stokes problems introducing the good behavior of the inf-sup and optimal energy estimates for the velocity and pressure. In addition, this method can treat a finite number of non-overlapping domains with non-matching grids at interfaces. In [16, 32, 52], Stokes system local discontinuous Galerkin methods for a class of shape regular meshes with hanging nodes is investigated, as well as, several mixed discontinuous Galerkin approximations with their a priori error estimates. In [6], a discontinuous Galerkin (dG) approach to simulations on complex-shaped domains, using trial and test functions defined on a structured grid with essential boundary conditions imposed weakly, where the discretization allows the number of unknowns to be independent of the complexity of the domain. [44] concerns an unfitted dG method proposing to discretize elliptic interface problems, where *h*- and *hp*- error estimates and convergence rates are proved. The authors of [56], treat an unfitted dG method for the elliptic interface problems, based on a variant of the local dG method, obtaining the optimal convergence for the exact solution in the energy norm and its flux in the L^2 norm. In [7] an unfitted discontinuous Galerkin method for transport processes in complex domains in porous media problems is examined, allowing finite element meshes that are significantly coarser than those required by standard conforming finite element approaches. Further, in [25] an advection problem is developed based on an unfitted discontinuous Galerkin approach where the surface is not explicitly tracked by the mesh which means the method is flexible with respect to geometry efficiently capturing the advection driven by the evolution of the surface without the need for a space-time formulation, back-tracking trajectories or streamline diffusion. Finally, in [24] a linear transport equation on a cut cell mesh using the upwind discontinuous Galerkin method with piecewise linear polynomials and with a method of lines approach is presented employing explicit time-stepping schemes, regardless of the presence of cut cells.

In addition, various classes of fitted and unfitted mesh methods for interface or transmission problems may be seen as generalized concepts of mesh elements, as well as, several unfitted finite element methods have been proposed in recent years, indicatively we mention the unfitted boundary finite element methods [5] and immersed finite element methods [41]. More extensively, an optimally convergent method of fictitious type domains avoiding the numerical integration on cut mesh elements for a Poisson system has been introduced in [40], while in [29] a method for the finite element solution of the elliptic interface problem, using an approach due to Nitsche is proposed allowing discontinuities internal to the elements approximating the solution across the interface. In addition, from a reduced basis for unfitted mesh methods point of view, evaluating the fixed background mesh used in immersed and unfitted mesh methods, parametrized Stokes and other flow systems have managed to be solved using a unified reduced basis presenting the flexibility of such methods in geometrically parametrized Stokes, Navier-Stokes, Cahn-Hilliard systems as in [33–37]. For an immersed interface method for discrete surface representations employing accurate jump conditions evaluated along interface representations using projections, one could see [38], and for a ghost fluid method coupled with a volume

of fluid method employing an exact Riemann solver [10]. For a fictitious domain finite element method, well suited for elliptic problems posed in a domain given by a level-set function without requiring a mesh fitting the boundary can be found in [23]. The early work of [50] handles the flow of a viscous incompressible fluid containing immersed boundaries which move with the fluid and exert forces on the fluid, and in [57] a finite difference scheme with ghost cell technique is used to study viscous fluid flow with internal structures. In [49], a conservative cut-cell Immersed Boundary method with sub-cell resolution is analyzed.

We extend the literature with [31], where a high-order hybridizable dG method for solving elliptic interface problems in which the solution and gradient are non-smooth because of jump conditions across the interface and it is endowed with several distinct characteristics. [19] contains an unfitted hybridizable dG method mesh method for the Poisson interface problem constructing an ansatz function in the vicinity of the interface with an appropriate choice of flux for treating the jump conditions, designed through a piecewise quadratic Hermite polynomial interpolation with post-processing via a standard Lagrange polynomial interpolation. These approaches usually employ penalization on the boundary interface and/or weak enforcement of the boundary conditions and data usually supported by a level set geometry description, [48].

In the present work, we investigate the applicability of the interior-penalty discontinuous Galerkin method discretizing steady Stokes flow cases onto meshes with boundaries considering general, essentially arbitrarily shaped element shapes in the sense of [13], which allow attaining smaller errors compared with other competitive finite element methods e.g. comparing with the unfitted dG approaches of [2], fact verified numerically in Section 6. Furthermore, our analysis allows for curved element shapes without the use of any non-linear elemental maps. We use extended *hp*- trace and inverse estimates to the arbitrary shape of boundary elements and we prove the inf-sup stability of the method in proper, to the prescribed method, norm. A priori error bounds for the resulting method are given under very weak assumptions. Numerical experiments are also presented, indicating the efficiency of the proposed framework.

This manuscript is structured as follows: we start with the Stokes flow model problem and the necessary preliminaries in Section 2. The various components of the interior penalty stabilized arbitrary boundary elements dG discretization are discussed in subsection 2.2 and we recall trace inverse estimates that are pivotal in the proof of the stability of IP-dG methods employed with the constants that appear and affect several inverse, stability, and error estimates. Approximation results needed for the analysis of the method are collected in Section 3. Section 4 is devoted to stability estimates and the derivation of the discrete inf–sup condition, followed by a–priori error estimates in Section 5. Concluding, the aforementioned analysis is numerically verified with tests in Section 6 that depict the optimal theoretical *hp*-convergence rates and the *hp*-accuracy of the method.

It is noted that this work determines an approach where many expensive penalization terms can be omitted and appear beneficial especially, for fluid systems where additional penalization is needed. These results are relevant to the *hp*-version framework and geometrical challenges and verify that there is no loss of stability and accuracy, as traditionally appears e.g. in cases with excessive and/or insufficient penalization that typically results in accuracy loss. Further, we report that the theoretical tools presented are adapted to a Nitsche-type formulation. The inf-sup stability result of the method in a Stokes-like norm is proved on *hp*-approximation

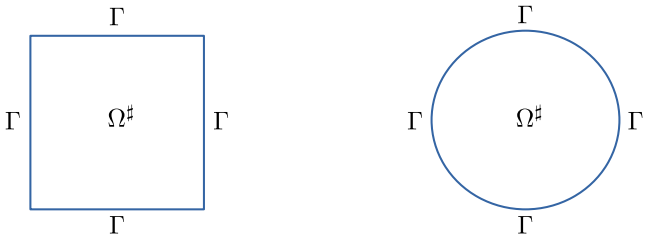

FIGURE 1. Example geometries $\Omega^\sharp$ and their boundaries Γ.

that will also lead to an error bound, an a priori error estimate and optimal convergence rates. The theoretical developments presented regarding stability and a-priori error analysis of IP-dG methods considering general arbitrarily shaped elements, to the best of our knowledge are new for Stokes systems.

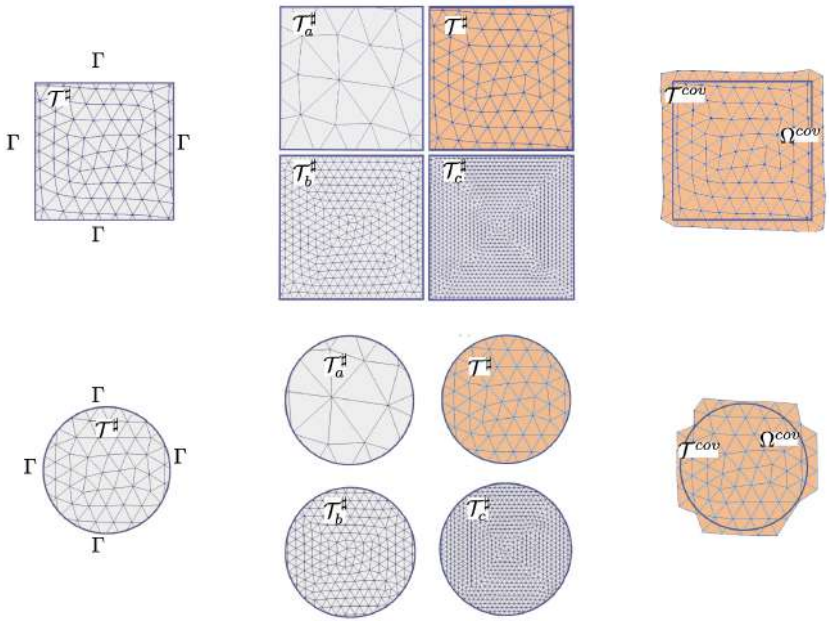

FIGURE 2. Meshes $\mathcal{T}^\sharp$ based on arbitrarily-shaped boundary elements, the covering meshes $\mathcal{T}^{cov}$ from Definition 3.7, examples of refined Figure 1's geometries $\Omega^\sharp$ tessellations $\mathcal{T}_a^\sharp$, $\mathcal{T}_b^\sharp$, $\mathcal{T}_c^\sharp$ and the covering domains, Ω^{cov}.

2. Model problem

2.1. Problem formulation. The steady Stokes equations for an incompressible viscous fluid confined in an open, bounded domain $\Omega^\sharp \subset \mathbb{R}^d$ $(d = 2, 3)$ with Lipschitz boundary $\Gamma = \partial\Omega^\sharp$ can be expressed in the form

$$-\Delta \mathbf{u} + \nabla p = \mathbf{f} \text{ and } \nabla \cdot \mathbf{u} = 0 \quad \text{in } \Omega^\sharp, \qquad \text{with} \qquad \mathbf{u} = 0 \quad \text{on } \Gamma. \tag{1}$$

Here $\mathbf{u} = (u_1, \ldots, u_d) : \Omega^\sharp \to \mathbb{R}^d$ $(d = 2, 3)$ and $p : \Omega^\sharp \to \mathbb{R}$ denote the velocity and pressure fields, and $\mathbf{f} \in \left[L^2(\Omega^\sharp)\right]^d$ is a forcing term. Since the pressure is determined by (1) up to an additive constant, we assume $\int_{\Omega^\sharp} p dx = 0$ to uniquely determine p. Hence, in the following, we will consider for pressure the standard space $L^2_0(\Omega^\sharp) := \left\{q \in L^2(\Omega^\sharp) : \int_{\Omega^\sharp} q\, dx = 0\right\}$ of square-integrable functions with zero average over $\Omega^\sharp$.

Defining for all $\mathbf{u}, \mathbf{v} \in V^\sharp := [H^1_0(\Omega^\sharp)]^d$ and $p \in Q^\sharp := L^2_0(\Omega^\sharp)$ the bilinear forms

$$a(\mathbf{u}, \mathbf{v}) = \int_{\Omega^\sharp} \nabla \mathbf{u} : \nabla \mathbf{v}\, d\boldsymbol{x}, \quad b(\mathbf{v}, p) = -\int_{\Omega^\sharp} p \nabla \cdot \mathbf{v}\, d\boldsymbol{x}, \tag{2}$$

a weak solution to (1) is a pair $(\mathbf{u}, p) \in [H^1_0(\Omega^\sharp)]^d \times L^2_0(\Omega^\sharp) = V^\sharp \times Q^\sharp$, such that

$$A(\mathbf{u}, p; \mathbf{v}, q) = \int_{\Omega^\sharp} \mathbf{f} \cdot \mathbf{v}\, d\boldsymbol{x}, \quad \text{for all test functions } (\mathbf{v}, q) \in V^\sharp \times Q^\sharp, \tag{3}$$

with

$$A(\mathbf{u}, p; \mathbf{v}, q) = a(\mathbf{u}, \mathbf{v}) + b(\mathbf{u}, q) + b(\mathbf{v}, p).$$

The well–posedness of (3) is standard [17].

2.2. Arbitrarily shaped discontinuous Galerkin method on the boundary. Implementation of arbitrarily shaped boundary elements discontinuous Galerkin method for the discretization of (3) relies on a covering domain Ω^{cov} which contains the true geometry $\Omega^\sharp$, see Figures 1, 2. Let $\mathcal{T}^{cov}$ be the corresponding covering shape-regular mesh of Ω^{cov} and $\mathcal{T}^\sharp$ is the mesh corresponding to $\Omega^\sharp$. The *active* mesh

$$\mathcal{T}^\sharp = \left\{\mathcal{K} \cap \Omega^\sharp;\ \text{for all } \mathcal{K} \in \mathcal{T}^{cov} \text{ with } \mathcal{K} \cap \Omega^\sharp \neq \emptyset\right\}$$

is the minimal submesh of $\mathcal{T}^{cov}$ which covers $\Omega^\sharp$ employing polytopic, e.g. polygonal boundary interface elements and is actually *fitted* to its boundary Γ: we allow mesh boundary elements $K \in \mathcal{T}^\sharp$ which are arbitrarily shaped and with very general interfaces. In the present work, numerical experiments consider boundary elements as Lipschitz curved elements and with only curved facet the one that coincides to the corresponding part of the boundary Γ, see Figures 1, 2 or the more general case of Figure 3. However, one could also employ general interfaces with neighboring elements, [14, 20, 22].

Finite element spaces for $\mathbf{u}$ and p will be built upon the domain $\Omega^\sharp = \bigcup_{K \in \mathcal{T}^\sharp} K$ which corresponds to $\mathcal{T}^\sharp$. The mesh skeleton $\bigcup_{K \in \mathcal{T}^\sharp} \partial K$ –including the curved boundary facets– is subdivided into the internal part

$$\mathcal{F}^\sharp_{int} = \left\{F = K^+ \cap K^- : K^+, K^- \in \mathcal{T}^\sharp \text{ and } F \nsubseteq \Gamma\right\}$$

which actually denotes the set of interior faces in the active mesh and the boundary part $\Gamma \equiv \partial\Omega^\sharp$. We denote by $h_K = diam(K)$ the *local* mesh size for $K \in \mathcal{T}^\sharp$ boundary elements and $h_F = \min\{h_{K^+}, h_{K^-}\}$ for $F = K^+ \cap K^-$.

We choose to enforce boundary conditions at Γ to be weakly satisfied through Nitsche's method. We highlight that we do not employ coercivity recovery techniques applied over the covering domain Ω^{cov}, e.g. by means of additional ghost penalty terms which act on the gradient jumps –usually higher order– in the boundary zone; see, for instance, [11, 12, 33, 42]. Instead, the $\mathcal{T}^\sharp$ coercivity is ensured following the approach of [14, 20].

To define the arbitrarily shape discontinuous Galerkin discretization for the Stokes problem (3), we employ the element-wise discontinuous polynomial finite

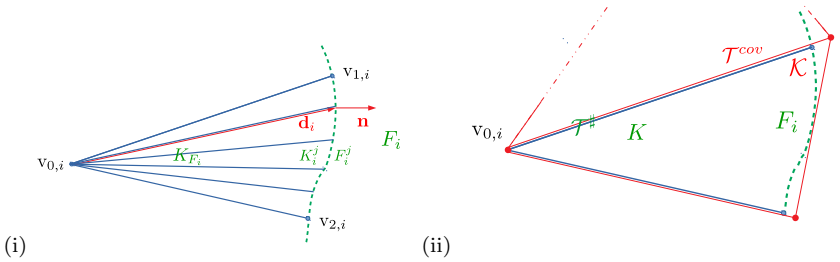

FIGURE 3. (i) Curved boundary elements for $d = 2$ with one curved face and vertices $\mathbf{v}_{k,i}$ and the unit outward normal vector to F_i at $x \in F_i$ where K_{F_i} is star-shaped and (ii) the covering mesh $\mathcal{T}^{cov}$, and the mesh $\mathcal{T}^\sharp$ corresponding to the truth geometry with arbitrary shape boundary elements.

elements for pressure and velocity spaces of order $\mathfrak{p} \geq 1$:

$$V_h^\sharp \equiv S^{\mathfrak{p}}_{\mathcal{T}^\sharp,\mathbf{u}_h} := \left\{ w_h \in \left(L^2(\Omega^\sharp)\right)^d : w_h|_K \in \left(\mathcal{P}^{\mathfrak{p}}(K)\right)^d, K \in \mathcal{T}^\sharp \right\} \quad (d = 2, 3)$$
$$Q_h^\sharp \equiv S^{\mathfrak{p}}_{\mathcal{T}^\sharp,p_h} := \left\{ w_h \in L^2_0(\Omega^\sharp) : w_h|_K \in \mathcal{P}^{\mathfrak{p}-1}(K), K \in \mathcal{T}^\sharp \right\}.$$

The broken Sobolev space $H^{\mathfrak{p}}(\Omega^\sharp, \mathcal{T}^\sharp)$, with respect to the subdivision $\mathcal{T}^\sharp$ up to composite order $\mathfrak{p}$, is defined as

$$H^{\mathfrak{p}}(\Omega^\sharp, \mathcal{T}^\sharp) = \{ w \in L^2(\Omega^\sharp) : w|_K \in H^{\mathfrak{p}}(K) \ \forall K \in \mathcal{T}^\sharp \}.$$

It is important to mention that whenever the notation ∇v is used for functions that lay in the discontinuous Galerkin space, i.e. $w \notin H^1(\Omega^\sharp)$, will correspond to the broken gradient, such that, $(\nabla w)|_K = \nabla(w|_K)$ for all $K \in \mathcal{T}^\sharp$. So, the broken gradient $\nabla_{\mathcal{T}^\sharp} w$ of a function $w \in L^2(\Omega^\sharp)$ with $w|_K \in H^1(K)$, for all $K \in \mathcal{T}$, is defined element-wise by $(\nabla_{\mathcal{T}^\sharp} w)|_K := \nabla(w|_K)$. When $F \subset \Gamma$, it is $\{\!\{w\}\!\} = [\![w]\!] = w$ and $\{\!\{\mathbf{w}\}\!\} = [\![\mathbf{w}]\!] = \mathbf{w}$. The same applies to the broken divergence operator $\nabla \cdot w$ defined element-wise. Moreover, recall the definition

$$\{\!\{w\}\!\} := \frac{1}{2}\left(w^+ + w^-\right), \qquad \{\!\{\mathbf{w}\}\!\} := \frac{1}{2}\left(\mathbf{w}^+ + \mathbf{w}^-\right),$$

of the *average* operator $\{\!\{\cdot\}\!\}$ across an interior face F for w, $\mathbf{w}$ scalar and vector-valued functions on $\mathcal{T}^\sharp$ respectively, where $w^\pm$ (resp. $\mathbf{w}^\pm$) are the traces of w (resp. $\mathbf{w}$) on $F = K^+ \cap K^-$ from the interior of $K^\pm$. More precisely, with $w^\pm(\mathbf{x}) = \lim_{t \to 0^+} w(\mathbf{x} \pm t\mathbf{n_F})$ for $\mathbf{x} \in F$ and $\mathbf{n_F}$ we denote the outward-pointing unit normal vector to F and with $\mathbf{n}_\Gamma$ the outward unit normal to the boundary Γ. The *jump* operator $[\![\cdot]\!]$ across F is defined respectively by

$$[\![w]\!] := w^+ - w^-, \qquad [\![\mathbf{w}]\!] := \mathbf{w}^+ - \mathbf{w}^-.$$

We are now ready to formulate a discrete counterpart of (3) through a discontinuous Galerkin method. The symmetric interior penalty discretizations of the

diffusion term and the pressure–velocity coupling in (2) lead to the bilinear forms

$$
\begin{aligned}
a_h(\mathbf{u}_h,\mathbf{v}_h) = &\int_{\Omega^\sharp} \nabla\mathbf{u}_h : \nabla\mathbf{v}_h \, d\boldsymbol{x} \\
&- \sum_{F\in\mathcal{F}^\sharp_{int}\cup\Gamma} \int_F \left(\{\!\{\nabla\mathbf{u}_h\}\!\}\cdot\mathbf{n_F}[\![\mathbf{v_h}]\!] + \{\!\{\nabla\mathbf{v_h}\}\!\}\cdot\mathbf{n_F}[\![\mathbf{u_h}]\!]\right) d\gamma \\
&- \int_\Gamma \mathbf{u}_h\nabla\mathbf{v}_h\cdot\mathbf{n}_\Gamma \, d\gamma - \int_\Gamma \mathbf{v}_h\nabla\mathbf{u}_h\cdot\mathbf{n}_\Gamma \, d\gamma + \int_\Gamma \sigma\mathbf{u}_h\mathbf{v}_h \, d\gamma \\
&+ \sum_{F\in\mathcal{F}^\sharp_{int}\cup\Gamma} \int_F \sigma[\![\mathbf{u}_h]\!][\![\mathbf{v}_h]\!] \, d\gamma, \\
b_h(\mathbf{v}_h,p_h) = &-\int_{\Omega^\sharp} p_h\nabla\cdot\mathbf{v}_h \, d\boldsymbol{x} + \sum_{F\in\mathcal{F}^\sharp_{int}\cup\Gamma}\int_F [\![\mathbf{v}_h]\!]\cdot\mathbf{n_F}\{\!\{p_h\}\!\} \, d\gamma + \int_\Gamma \mathbf{v}_h\cdot\mathbf{n_\Gamma}p_h \, d\gamma,
\end{aligned}
$$

where $\sigma > 0$ is the discontinuity-penalization function in $L^\infty(\mathcal{F}^\sharp_{int}\cup\Gamma)$ that affects the stability of the method as well as the approximation quality and will be investigated below. This symmetric interior penalty parameter in the definition of $a_h(\cdot,\cdot)$ will be sufficiently large in a sense that will be made precise later, see Lemma 4.2 and its proof below.

We note that the latter formulation's disadvantage is that it is not well defined for $H^1(\Omega^\sharp)$ regularity, e.g. traces of functions defined in $L^2(\Omega^\sharp)$ are not well defined in $\mathcal{F}^\sharp_{int}$. The latter issue affects the terms $\{\!\{\nabla(w)\}\!\}$, and $\nabla w\cdot\mathbf{n}_F$ in the sense that they are not well defined in $H^1(\Omega^\sharp)$. This causes the need of additional regularity while the Galerkin orthogonality cannot be derived explicitly. In order to achieve optimal a priori error estimates, under the presence of terms such $\{\!\{\nabla w\}\!\}|_F$, $\nabla w\cdot\mathbf{n}_F|_F$ which may involve $\{\!\{\nabla(w-\pi_\mathfrak{p}w)\}\!\}_F$ and $\nabla(w-\pi_\mathfrak{p}w)\cdot\mathbf{n}_F|_F$, where $\pi_\mathfrak{p}w$ is an operator $\pi_\mathfrak{p} : H^{l_\mathcal{K}}(\mathcal{K}) \to \mathcal{P}_\mathfrak{p}(\mathcal{K})$ an approximation of w for $l_k \geq 0$ will be introduced in Lemma 4.3 and it is estimated optimally. We note at this point that the $H^1(F)$ semi-norm for an *hp*- a priori approximation error bound would require $W^{1,\infty}$ norm error bounds which also require further regularity, see for more details the work of [14]. To avoid the latter issue we employ proper bilinear form extensions. In particular we introduce the orthogonal L^2-projection in the FEM space $S^\mathfrak{p}_{\mathcal{T}^\sharp,\cdot}$, e.g. $\mathbf{\Pi}_{L^2} : (L^2(\Omega^\sharp))^d \to (S^\mathfrak{p}_{\mathcal{T}^\sharp,\cdot})^d$ concluding in the variational form:

$$
\begin{aligned}
\widetilde{a}_h(\mathbf{u}_h,\mathbf{v}_h) = &\int_{\Omega^\sharp} \nabla\mathbf{u}_h : \nabla\mathbf{v}_h \, d\boldsymbol{x} \\
&- \sum_{F\in\mathcal{F}^\sharp_{int}\cup\Gamma} \int_F \left(\{\!\{\mathbf{\Pi_{L^2}}(\nabla\mathbf{u}_h)\}\!\}\cdot\mathbf{n_F}[\![\mathbf{v_h}]\!] + \{\!\{\mathbf{\Pi_{L^2}}(\nabla\mathbf{v_h})\}\!\}\cdot\mathbf{n_F}[\![\mathbf{u_h}]\!]\right) d\gamma \\
&- \int_\Gamma \mathbf{u}_h\mathbf{\Pi_{L^2}}(\nabla\mathbf{v}_h)\cdot\mathbf{n}_\Gamma \, d\gamma - \int_\Gamma \mathbf{v}_h\mathbf{\Pi_{L^2}}(\nabla\mathbf{u}_h)\cdot\mathbf{n}_\Gamma \, d\gamma \\
&+ \int_\Gamma \sigma\mathbf{u}_h\mathbf{v}_h \, d\gamma + \sum_{F\in\mathcal{F}^\sharp_{int}\cup\Gamma} \int_F \sigma[\![\mathbf{u}_h]\!][\![\mathbf{v}_h]\!] \, d\gamma, \\
b_h(\mathbf{v}_h,p_h) = &-\int_{\Omega^\sharp} p_h\nabla\cdot\mathbf{v}_h \, d\boldsymbol{x} + \sum_{F\in\mathcal{F}^\sharp_{int}\cup\Gamma}\int_F [\![\mathbf{v}_h]\!]\cdot\mathbf{n_F}\{\!\{p_h\}\!\} \, d\gamma + \int_\Gamma \mathbf{v}_h\cdot\mathbf{n_\Gamma}p_h \, d\gamma
\end{aligned}
$$

respectively. For future reference, note that element-wise integration by parts in the previous forms yields the equivalent formulations

$$\begin{aligned}\widetilde{a}_h(\mathbf{u}_h,\mathbf{v}_h) =& -\int_{\Omega^\sharp}\nabla\nabla\mathbf{u}_h\cdot\mathbf{v}_h\,d\boldsymbol{x}+\sum_{F\in\mathcal{F}^\sharp_{int}\cup\Gamma}\int_F[\![\boldsymbol{\Pi}_{\mathbf{L^2}}(\nabla\mathbf{u}_h)]\!]\cdot\mathbf{n}_{\mathbf{F}}\,\{\!\{\mathbf{v}_h\}\!\}\,d\gamma\\ &-\sum_{F\in\mathcal{F}^\sharp_{int}\cup\Gamma}\int_F\{\!\{\boldsymbol{\Pi}_{\mathbf{L^2}}(\nabla\mathbf{v}_h)\}\!\}\cdot\mathbf{n}_{\mathbf{F}}[\![\mathbf{u}_h]\!]\,d\gamma-\int_\Gamma\mathbf{u}_h\boldsymbol{\Pi}_{\mathbf{L^2}}(\nabla\mathbf{v}_h)\cdot\mathbf{n}_\Gamma\,d\gamma\\ &+\int_\Gamma\sigma\mathbf{u}_h\mathbf{v}_h\,d\gamma+\sum_{F\in\mathcal{F}^\sharp_{int}\cup\Gamma}\int_F\sigma[\![\mathbf{u}_h]\!][\![\mathbf{v}_h]\!]\,d\gamma,\end{aligned}\tag{4}$$

and

$$b_h(\mathbf{v}_h,p_h)=\int_{\Omega^\sharp}\mathbf{v}_h\cdot\nabla p_h\,d\boldsymbol{x}-\sum_{F\in\mathcal{F}^\sharp_{int}\cup\Gamma}\int_F\{\!\{\mathbf{v}_h\}\!\}\cdot\mathbf{n}_{\mathbf{F}}[\![p_h]\!]\,d\gamma,\tag{5}$$

which will be useful for asserting the consistency of the method.

Using the aforementioned weak formulation, an arbitrarily shape boundary elements discontinuous Galerkin method for (3) now reads as follows: Find $(\mathbf{u}_h,p_h)\in V_h^\sharp\times Q_h^\sharp$, such that

$$A_h(\mathbf{u}_h,p_h;\mathbf{v}_h,q_h)=L_h(\mathbf{v}_h,q_h),\quad\text{for all}\quad(\mathbf{v}_h,q_h)\in V_h^\sharp\times Q_h^\sharp.\tag{6}$$

The bilinear and linear forms A_h and L_h are defined by

$$\begin{aligned}A_h(\mathbf{u}_h,p_h;\mathbf{v}_h,q_h)=&\widetilde{a}_h(\mathbf{u}_h,\mathbf{v}_h)+b_h(\mathbf{u}_h,q_h)+b_h(\mathbf{v}_h,p_h),\\ \text{and}\quad L_h(\mathbf{v}_h,q_h)=&\int_{\Omega^\sharp}\mathbf{f}\cdot\mathbf{v}_h\,d\boldsymbol{x}.\end{aligned}\tag{7}$$

We report that in the right-hand side $L_h(\mathbf{v}_h,q_h)$ we have omitted the zero Nitsche boundary terms, as well as, $\widetilde{a}_h(\mathbf{u}_h,\mathbf{v}_h)=a_h(\mathbf{u}_h,\mathbf{v}_h)$ when $\mathbf{u}_h,\mathbf{v}_h\in V_h^\sharp$.

3. Preliminaries

Next, we define the discontinuity penalization parameter $\sigma:\Gamma\cup\mathcal{F}^\sharp_{int}\to\mathbb{R}$, the standard Sobolev norms and semi–norms on a domain $\mathcal{X}$ for $s\in\mathbb{N}$ will be denoted by $\|\cdot\|_{s,\mathcal{X}}$ and $|\cdot|_{s,\mathcal{X}}$, respectively, omitting the index in case $s=0$. The a–priori error bounds for the proposed dG method will be proved with respect to the following mesh-dependent norms:

$$\begin{aligned}|||\mathbf{v}|||^2=&\|\nabla\mathbf{v}\|^2_{\Omega^\sharp}+\|\sigma^{1/2}\mathbf{v}\|^2_\Gamma+\sum_{F\in\Gamma}\|\mathfrak{p}^{-1}h_F^{1/2}\nabla\mathbf{v}\cdot\mathbf{n}_\Gamma\|^2_F\\ &+\sum_{F\in\mathcal{F}^\sharp_{int}}\|\sigma^{1/2}[\![\mathbf{v}]\!]\|^2_F+\frac{1}{2}\sum_{K\in\mathcal{T}^{cov}}\|\mathfrak{p}^{-1}h_K^{1/2}\nabla\mathbf{v}|_T\cdot\mathbf{n}_T\|^2_{\partial K},\\ |||p|||^2=&\|p\|^2_{\Omega^\sharp}+\sum_{F\in\Gamma}\|\mathfrak{p}^{-1}h_F^{1/2}p\|^2_F+\sum_{F\in\mathcal{F}^\sharp_{int}}\|\mathfrak{p}^{-1}h_F^{1/2}[\![p]\!]\|^2_F\\ &+\frac{1}{2}\sum_{K\in\mathcal{T}^{cov}}\|\mathfrak{p}^{-1}h_K^{1/2}p\|^2_{\partial K},\end{aligned}$$

and $|||(\mathbf{v},p)|||^2=|||\mathbf{v}|||^2+|||p|||^2$. To investigate stability, since some terms of the above terms dominate related to others, we will also make use of the following norms in $\Omega^\sharp$ for the discrete velocity and pressure approximations, e.g. for the velocity norm the third and fifth terms appear similar *hp*- behavior with the first

term and for pressure the second, third and fourth term with the first term. For this reason, we also update and define the norms:

$$|||(\mathbf{v})|||^2_{V^c} = \|\nabla \mathbf{v}\|^2_{\Omega^{cov}} + \|\sigma^{1/2}\mathbf{v}\|^2_{\Gamma} + \sum_{F\in\mathcal{F}^{\sharp}_{int}} \|\sigma^{1/2}[\![\mathbf{v}]\!]\|^2_{F}, \quad \text{and} \quad |||p|||^2_{Q^c} = \|p\|^2_{\Omega^{cov}},$$

while $|||(\mathbf{v},p)|||^2_{V^c,Q^c} = |||\mathbf{v}|||^2_{V^c} + |||p|||^2_{Q^c}$. We underline, that in the following, and for completeness we treat all the aforementioned terms showing this equivalence.

The following section is devoted to useful trace and inverse estimates, which have been proved in [14,20] and they will form the basis to prove a–priori error estimates of the proposed method.

3.1. Inverse estimates (trace and H^1–L^2). It is easy to derive the estimates with respect to the norms $|||\cdot|||$ and $|||\cdot|||_{V^c \text{ or } Q^c}$, namely,

$$|||\mathbf{v}||| \leq C_{V^c}|||\mathbf{v}|||_{V^c}, \quad |||p||| \leq C_{Q^c}|||p|||_{Q^c}. \tag{9}$$

Assumption 3.1. *For each element $K \in \mathcal{T}^{\sharp}$ with $K\cap\Gamma \neq \emptyset$, we assume that K is a Lipschitz domain, and ∂K can be subdivided into mutually exclusive subsets $\{F_i\}_{i=1}^{n_K}$ characterized by the property that respective sub-elements $K_{F_i} \equiv K_{F_i}(v_{0,i}) \subset K$ there exist, with d planar faces meeting at one vertex $v_{0,i} \in K$, with $F_i \subset \partial K_{F_i}$: for $i = 1, ..., n_K$, we consider that (a) K_{F_i} is star-shaped with respect to $v_{0,i}$, and (b) $\mathbf{d}_i(x)\cdot\mathbf{n}_{F_i}(x) > 0$ for $\mathbf{d}_i(x) := x - v_{0,i}$, $x \in K_{F_i}$, and $\mathbf{n}_{F_i}(x)$ the respective unit outward normal vector to F_i at $x \in F_i$. It is also considered that the boundary ∂K of each element $K \in \mathcal{T}^{\sharp}$, $K \cap \Gamma \neq \emptyset$ is the union of a finite number of closed C^1 surfaces.*

Both (a) and (b) assumptions, for the two-dimensional case, are visualized in Figure 3. We notice that in the above weak mesh assumption, the sub-domains $\{F_i\}_{i=1}^{n_K}$ are not required to coincide with the faces of the element K, namely, each F_i may be part of a face or may include one or more faces of K, as well as, there is no requirement for $\{n_K\}_{K\in\mathcal{T}^{\sharp},K\cap\Gamma\neq 0}$ to remain uniformly bounded across the mesh. In particular Assumption 3.1 states that the curvature of the collection of consecutive curved faces comprising F_i cannot be arbitrarily large almost everywhere. Moreover, with some small loss of generality, Assumption 3.1 b) can be made stronger by adding the ingredient that it is possible to consider a fixed point $\mathrm{v}_{0,i}$ such that there exists a global constant $c_{sh} > 0$, such that

$$\mathbf{d}_i(x)\cdot\mathbf{n}_{F_i}(x) \geq c_{sh}h_{K_{F_i}} \tag{10}$$

see e.g. [24, 65]. We underline that (10) does not imply shape-regularity of the K_{F_i}'s; in particular K_{F_i}'s with small F_i compared to the remaining (straight) faces of K_{F_i} are acceptable. Such anisotropic boundary sub-elements K_{F_i}'s may be necessary to ensure that each K_{F_i} remains star-shaped when an element boundary's curvature is locally large, see e.g., K_{F_i} in Figure 3 and a collection of both shape-regular and anisotropic K_{F_i}'s. In general, F_i is not required to be connected, although, by splitting F_i to its connected subsets, re-indexing the F_i's to correspond to unique K_{F_i}, we can correspond one K_{F_i} to each F_i. The aforementioned Assumptions 3.1 are sufficient for the proof of the trace estimates as well as for the validity of the H^1–L^2 inverse estimate as in [14].

Lemma 3.2. *Let element $K \in \mathcal{T}^{\sharp}$ be a Lipschitz domain satisfying Assumption 3.1. Then, for each $F_i \subset \partial K$ from Assumptions 3.1, $i = 1, ..., n_K$, and for each*

$v \in \mathcal{P}^{\mathfrak{p}}(K)$, we have the inverse estimate:

$$||v||^2_{F_i} \leq \frac{(\mathfrak{p}+1)(\mathfrak{p}+d)}{\min\limits_{x\in F_i}(\mathbf{d}_i \cdot \mathbf{n}_{F_i})}||v||^2_{K_{F_i}}. \tag{11}$$

Remark 3.3. Inequality (11) is a function of $\mathrm{v}_{0,i}$ defining K_{F_i}. The right-hand side can be minimized with a choice of an optimal $\mathrm{v}_{0,i}$. We underline that under the stronger assumption (3.1), one could derive the trace inverse estimate for star-shaped, shape-regular elements with piece-wise smooth boundaries: $||v||^2_{\partial K} \leq C\frac{\mathfrak{p}^2}{h_K}||v||^2_K$.

Lemma 3.4. *Let $K \in \mathcal{T}^\sharp$ be a Lipschitz domain satisfying Assumption 3.1. Then, for all $\varepsilon > 0$, we have the estimate*

$$||v||^2_{F_i} \leq \frac{d+\varepsilon}{\min\limits_{x\in F_i}(\mathbf{d}_i \cdot \mathbf{n}_{F_i})}||v||^2_{K_{F_i}} + \frac{\max\limits_{x\in F_i}|\mathbf{d}_i|_2^2}{\varepsilon \min\limits_{x\in F_i}(\mathbf{d}_i \cdot \mathbf{n}_{F_i})}||\nabla v||^2_{K_{F_i}},$$

for all $v \in H^1(\Omega^\sharp)$ and $i = 1, ..., n_K$. We note that summing over $i = 1, ..., n_K$, under assumption $\mathbf{d}_i(x)\cdot\mathbf{n}_{F_i}(x) \geq c_{sh}h_{K_{F_i}}$ and that $h_{K_{F_i}} \sim h_K$ we take the estimate gives the classical trace estimate $||v||^2_{\partial K} \leq C(h_K^{-1}||v||^2_K + h_K||\nabla v||^2_K)$.

Definition 3.5. An element $K \in \mathcal{T}^\sharp$ is said to be $\mathfrak{p}$-coverable with respect to $\mathfrak{p} \in \mathbb{N}$, if there exists a set of m_K overlapping shape regular simplices K_i, $i = 1, ..., m_K$, $m_K \in \mathbb{N}$, such that

$$dist(K, \partial K_i) < C_{\mathrm{as}}\frac{\mathrm{diam}(K_i)}{\mathfrak{p}^2}, \text{ and } |K_i| \geq c_{\mathrm{as}}|K| \tag{12}$$

for all $i = 1, ..., m_K$, where C_{as} and c_{as} are positive constants, independent of K and $\mathcal{T}^\sharp$.

Lemma 3.6 ([14])**.** *Let $K \in \mathcal{T}^\sharp$ Lipschitz satisfying Assumption 3.1. Then, for each $v \in \mathcal{P}^{\mathfrak{p}}(K)$, we have the inverse inequality*

$$||v||^2_{F_i} \leq C_{INV}(\mathfrak{p}, K, F_i)\frac{(\mathfrak{p}+1)(\mathfrak{p}+d)|F_i|}{|K|}||v||^2_K, \tag{13}$$

with $C_{INV}(\mathfrak{p}, K, F_i)$ to be if K is $\mathfrak{p}$-coverable: $\min\{\mathcal{C}(K, F_i), c_{as}^{-1}2^{5d+1}\mathfrak{p}^{2(d-1)}\}$, otherwise:
$\mathcal{C}(K, F_i)$, with $c_{as} > 0$ as in Definition 3.5 and $\mathcal{C} = \frac{|K|}{|F_i|\sup\limits_{\mathbf{v}_{0,i}\in K}\min\limits_{\mathbf{x}\in F_i}(\mathbf{d}_i\cdot\mathbf{n}_{F_i})}$.

After defining the covering domain $\bar{\Omega}^{cov}$ and considering the Assumption 3.8, see e.g. [14, 20], we interpolate a pair $(\mathbf{u}, p) \in [H^2(\Omega^\sharp)]^d \times H^1(\Omega^\sharp)$ through a suitable interpolant of $[H^{\mathfrak{p}+1}(\Omega^\sharp)]^d \times H^{\mathfrak{p}}(\Omega^\sharp)$ -extensions of the functions $(\mathbf{u}, p)$ on Ω^{cov}.

Definition 3.7. Given a mesh $\mathcal{T}^\sharp$, we define a covering $\mathcal{T}^{cov} = \{\mathcal{K}\}$ of $\mathcal{T}^\sharp$ to be a set of open shape-regular dCsimplices $\mathcal{K}$, such that for each $K \in \mathcal{T}^\sharp$, there exists a $\mathcal{K} \in \mathcal{T}^{cov}$ with $K \subset \mathcal{K}$. For a given $\mathcal{T}^{cov}$, we define the covering domain $\bar{\Omega}^{cov} := \cup_{\mathcal{K}\in\mathcal{T}^{cov}}\bar{\mathcal{K}}$.

Assumption 3.8. *For a given mesh $\mathcal{T}^\sharp$, we postulate the existence of a covering $\mathcal{T}^{cov}$, and of a global constant $\mathcal{O}_{\Omega^\sharp} \in \mathbb{N}$, independent of the mesh parameters, such that*

$$\max_{K\in\mathcal{T}} card\{K' \in \mathcal{T} : K' \cup \mathcal{K} \neq \emptyset, \mathcal{K} \in \mathcal{T}^{cov} \text{ such that } K \subset \mathcal{K}\} \leq \mathcal{O}_{\Omega^\sharp}.$$

For such $\mathcal{T}^{cov}$, we further assume that $h_{\mathcal{K}} := diam(\mathcal{K}) \leq C_{diam} h_K$, for all pairs $K \in \mathcal{T}^{\sharp}$, $\mathcal{K} \in \mathcal{T}^{cov}$, with $K \subset \mathcal{K}$, for a global constant $C_{diam} > 0$, uniformly with respect to the mesh size h_K.

The latter assumption provides the shape-regularity of the covering mesh $\mathcal{T}^{cov}$ –not though for the true $\mathcal{T}^{\sharp}$– in the sense that there exists a positive constant c, independent of the mesh parameters, such that $\forall K \in \mathcal{T}^{cov} \subset \mathcal{T}$, $\rho_{\mathcal{K}} \geq c h_{\mathcal{K}}$ holds, with $\rho_{\mathcal{K}}$ denoting the diameter of the largest ball contained in $\mathcal{K}$. The aforementioned will allow the application of the standard *hp*-version approximation estimates on simplicial elements, see e.g., from [53] that on each $\mathcal{K}$ we can restrict the error over $K \subset \mathcal{K}$. However, it requires to extend properly the exact solution u onto Ω^{cov}. In particular:

Theorem 3.9. *Let $\Omega^{\sharp}$ be a domain with a Lipschitz boundary. Then there exists a linear extension operator $\mathfrak{E} : H^s(\Omega^{\sharp}) \to H^s(\mathbb{R}^d)$, $s \in \mathbb{N}_0$, such that $\mathfrak{E}v|_{\Omega^{\sharp}} = v$ and*

$$||\mathfrak{E}v||_{H^s(\mathbb{R}^d)} \leq C_{\mathfrak{E}} ||v||_{H^s(\Omega^{\sharp})},$$

where $C_{\mathfrak{E}}$ is a positive constant depending only on s and on $\Omega^{\sharp}$.

We also recall from [14] the H^1–L^2 inverse inequality for polynomials on a general curved element $K \in \mathcal{T}^{\sharp}$.

Lemma 3.10. *Let $K \in \mathcal{T}^{\sharp}$ satisfy Assumptions 3.1, 3.8 and (10). Then, for each $v \in \mathcal{P}^{\mathfrak{p}}(K)$, the inverse estimates hold, for K $\mathfrak{p}$-coverable:*

$$||\nabla v||_K \leq C \frac{\mathfrak{p}^2}{h_K} ||v||_K, \text{ and} \tag{14}$$

$$||\nabla v \cdot \mathbf{n}_F||_F \leq C' \frac{\mathfrak{p}^3}{h_K^{3/2}} ||v||_K \tag{15}$$

hold, and the constants C, C' are dependent on the shape-regularity constant.

Proof. The first estimate comes immediately from [14] will the second comes from the algebraic calculations:

$$||\nabla v \cdot \mathbf{n}_F||_F \leq C \frac{\mathfrak{p}}{h_K^{1/2}} ||\nabla v||_K \leq C' \frac{\mathfrak{p}^2}{h_K} \frac{\mathfrak{p}}{h_K^{1/2}} ||v||_K = C' \frac{\mathfrak{p}^3}{h_K^{3/2}} ||v||_K.$$

□

4. Stability estimates

The fact that the discrete problem is well-posed follows by the inf–sup stability of the bilinear form A_h in the formulation (6) with respect to the $|||\cdot|||_{V^c,Q^c}$ norm. We begin by investigating the properties of the separate forms which contribute to A_h. A useful observation is that the form $\widetilde{a}_h(\cdot,\cdot)$, is continuous and coercive with respect to the norm $|||\cdot|||_{V^c}$. For this proof, we will use that the arbitrarily shaped boundary elements can be properly extended from the real domain $\Omega^{\sharp}$ to the covering one, Ω^{cov}.

Lemma 4.1. *There are constants $C_u, C_p > 0$, depending only on the shape-regularity and the polynomial order and not on the mesh or the location of the boundary, such that the following estimates hold:*

$$\|\nabla \mathbf{v_h}\|^2_{\Omega^{cov}} \leq C_u \|\nabla \mathbf{v}_h\|^2_{\Omega^{\sharp}} \leq C_u \|\nabla \mathbf{v}_h\|^2_{\Omega^{cov}}, \quad \text{for all } \mathbf{v}_h \in V_h^{\sharp}, \text{ and} \tag{16}$$

$$\|p_h\|^2_{\Omega^{cov}} \leq C_p \|p_h\|^2_{\Omega^{\sharp}} \leq C_p \|p_h\|^2_{\Omega^{cov}}, \quad \text{for all } p_h \in Q_h^{\sharp}. \tag{17}$$

Proof. Considering also the Assumption 3.1, we assume that there is an integer $N > 0$ such that for each element $K \in \mathcal{T}^{cov}$ with $K \cap \Gamma \neq \emptyset$ there exists an element $K' \in \mathcal{T}^{cov}$ with $K' \cap \Gamma = \emptyset$ and at most N elements $\{K\}_{i=1}^{N}$ such that $K_1 = K$, $K_N = K'$ and $K_i \cap K_{i+1} \in \partial_i \mathcal{T}^{cov}$, $i = 1, ...N-1$. In particular, this means that the number of facets we need to cross so that we pass from the aforementioned element K to $K' \subset \Omega^\sharp$ is bounded. Similar assumptions were made by [2], see also references therein, which ensure that Γ is reasonably resolved by $\mathcal{T}^{cov}$. For the first inequality (16) we compose the norm over Ω^{cov} into sums over internal and boundary $\mathcal{T}^{cov}$ elements, $\|\cdot\|_{\mathcal{T}^{cov}} = \sum \|\cdot\|_{\mathcal{T}^{cov}\text{-boundary-}K\text{'s}} + \sum \|\cdot\|_{\mathcal{T}^{cov}\text{-internal } K\text{'s}}$. Let K_0 be a boundary element of $\mathcal{T}^{cov}$. Then, there exists a $K_N \subset \Omega^\sharp$ and at most $N-1$ $\mathcal{T}^{cov}$-boundary elements K_i and facets $K_{i-1} \cap K_i = F_i$ that has to be overtaken in order to go across from K_0 to K_N. Considering the aforementioned shape-regularity of the mesh, each facet corresponding to $\mathcal{T}^{cov}$-boundary elements F will only be involved in a finite number of such crossings. Additionally, let v be a polynomial function of order $\mathfrak{p}$ defined on both the boundary element $K \in \mathcal{T}^\sharp$ and its corresponding extended $\mathcal{K} \in \mathcal{T}^{cov}$. Then there is a constant $C > 0$, depending only on the shape-regularity of $\mathcal{T}^{cov}$ and the polynomial order $\mathfrak{p}$ of v, such that $\|v\|_{\mathcal{K}}^2 \leq C\|v\|_K^2$. Here, each component of $\nabla \boldsymbol{v}_h$ has been treated as v iteratively to each neighboring pair $\{K_{i-1}, K_i\}$ and we take the desired estimate. The first inequality of (17) follows similarly following the same procedure for q_h. The second inequalities of (16)-(17) can be derived straightforwardly. □

With this preliminary result in place, we are now ready to prove discrete coercivity of $\widetilde{a}_h$ and continuity:

Lemma 4.2. *For suitably large discontinuity penalization parameter $\sigma > 0$ in the definition of the bilinear form $a_h(\cdot,\cdot)$, there exists a constant $c_a > 0$, such that*

$$\widetilde{a}_h(\mathbf{v}_h, \mathbf{v}_h) \geq c_{coer} |||\mathbf{v}_h|||_{V^\sharp}^2, \tag{18}$$

for any $\mathbf{v}_h \in V_h^\sharp$, and there exist constants $C_a, C_b > 0$, such that

$$\widetilde{a}_h(\mathbf{u}_h, \mathbf{v}_h) \leq C_a |||\mathbf{u}_h||| \cdot |||\mathbf{v}_h|||, \tag{19}$$

for every $\mathbf{u}_h, \mathbf{v}_h \in V_h^\sharp$,

$$\widetilde{a}_h(\mathbf{u}, \mathbf{v}_h) \leq C_a |||\mathbf{u}||| \cdot |||\mathbf{v}_h|||, \tag{20}$$

for every $(\mathbf{u}, \mathbf{v}_h) \in ([H^{k+1}(\Omega^\sharp) \cap H_0^1(\Omega^\sharp)]^d + V_h^\sharp) \times V_h^\sharp$,

$$b_h(\mathbf{u}, p_h) \leq C_b |||\mathbf{u}||| \cdot |||p_h|||, \tag{21}$$

for every $(\mathbf{u}, p_h) \in ([H^{k+1}(\Omega^\sharp) \cap H_0^1(\Omega^\sharp)]^d + V_h^\sharp) \times Q_h^\sharp$, and

$$b_h(\mathbf{u}_h, p) \leq C_b |||\mathbf{u}_h||| \cdot |||p|||, \tag{22}$$

for every $(\mathbf{u}_h, p) \in V_h^\sharp \times ([H^k(\Omega^\sharp) \cap L_0^2(\Omega^\sharp)] + Q_h^\sharp)$.

Proof. The proof is based on standard arguments. In particular, for any $\lambda > 0$, we have

$$
\begin{aligned}
\widetilde{a}_h(\mathbf{v}_h, \mathbf{v}_h) =& \|\nabla \mathbf{v}_h\|^2_{\Omega^\sharp} + \|\sigma^{1/2}\mathbf{v}_h\|^2_\Gamma + \sum_{F\in\mathcal{F}^\sharp_{int}} \|\sigma^{1/2}[\![\mathbf{v}_h]\!]\|^2_F \\
&- 2\int_\Gamma \mathbf{v}_h \boldsymbol{\Pi}_{\mathbf{L^2}}(\nabla \mathbf{v}_h)\cdot \mathbf{n}_\Gamma \, d\gamma - 2\sum_{F\in\mathcal{F}^\sharp_{int}} \int_F \{\!\{\boldsymbol{\Pi}_{\mathbf{L^2}}(\nabla \mathbf{v}_h)\}\!\}\cdot \mathbf{n}_F [\![\mathbf{v}_h]\!] \, d\gamma \\
\geq& \|\nabla \mathbf{v}_h\|^2_{\Omega^\sharp} + \|\sigma^{1/2}\mathbf{v}_h\|^2_\Gamma + \sum_{F\in\mathcal{F}^\sharp_{int}} \|\sigma^{1/2}[\![\mathbf{v}_h]\!]\|^2_F \\
&- \lambda\sigma\|\sigma^{-1/2}\boldsymbol{\Pi}_{\mathbf{L^2}}(\nabla \mathbf{v}_h)\cdot\mathbf{n}_\Gamma\|^2_\Gamma - \lambda^{-1}\sigma^{-1}\|\sigma^{1/2}\mathbf{v}_h\|^2_\Gamma \\
&- \lambda\sigma \sum_{F\in\mathcal{F}^\sharp_{int}} \|\sigma^{-1/2}\{\!\{\boldsymbol{\Pi}_{\mathbf{L^2}}(\nabla \mathbf{v}_h)\}\!\}\cdot\mathbf{n}_F\|^2_F - \lambda^{-1}\sigma^{-1}\sum_{F\in\mathcal{F}^\sharp_{int}} \|\sigma^{1/2}[\![\mathbf{v}_h]\!]\|^2_F \\
\geq& \|\nabla \mathbf{v}_h\|^2_{\Omega^\sharp} + (1-\lambda^{-1}\sigma^{-1})(\|\sigma^{1/2}\mathbf{v}_h\|^2_\Gamma + \sum_{F\in\mathcal{F}^\sharp_{int}} \|\sigma^{1/2}[\![\mathbf{v}_h]\!]\|^2_F) \\
&- \lambda\sigma(\sum_{F\in\mathcal{F}^\sharp_{int}} \|\sigma^{-1/2}\{\!\{\boldsymbol{\Pi}_{\mathbf{L^2}}(\nabla \mathbf{v}_h)\}\!\}\cdot\mathbf{n}_F\|^2_F + \|\sigma^{-1/2}\boldsymbol{\Pi}_{\mathbf{L^2}}(\nabla \mathbf{v}_h)\cdot\mathbf{n}_\Gamma\|^2_\Gamma). \qquad (23)
\end{aligned}
$$

Young's inequality $ab \leq a^2/(2\epsilon) + \epsilon b^2/2$ and inverse estimates (13), (15), are applied to the latter term in (23) to achieving a lower bound. In particular, note for $F \in \mathcal{F}^\sharp_{int}$ with $F = \partial K \cap \partial K^{'}$ that

$$
\begin{aligned}
&\|\sigma^{-1/2}\{\!\{\boldsymbol{\Pi}_{\mathbf{L^2}}(\nabla \mathbf{v}_h)\}\!\}\cdot\mathbf{n}_F\|_F \\
\leq& \frac{(\|\sigma^{-1/2}\boldsymbol{\Pi}_{\mathbf{L^2}}(\nabla \mathbf{v}_h)\cdot\mathbf{n}_F\|_{F\subset\partial K} + \|\sigma^{-1/2}\boldsymbol{\Pi}_{\mathbf{L^2}}(\nabla \mathbf{v}_h)\cdot\mathbf{n}_F\|_{F\subset\partial K'})}{2} \\
\leq& \mathfrak{p}^2 \left(C_{INV}(\mathfrak{p}, K, F_i)\frac{|F_i|}{|K|}||\boldsymbol{\Pi}_{\mathbf{L^2}}(\sigma^{-1/2}\nabla \mathbf{v}_h)\cdot\mathbf{n}_F||^2_K \right. \\
&\left. + C_{INV}(\mathfrak{p}, K', F_i)\frac{|F_i|}{|K'|}||\boldsymbol{\Pi}_{\mathbf{L^2}}(\sigma^{-1/2}\nabla \mathbf{v}_h)\cdot\mathbf{n}_F||^2_{K'} \right) \Big/ 2 \\
\leq& \frac{1}{2}\mathfrak{p}^2 \max_{\kappa=K,K'}\{C_{INV}(\mathfrak{p}, \kappa, F_i)\frac{|F_i|}{|\kappa|}\|\sigma^{-1/2}\boldsymbol{\Pi}_{\mathbf{L^2}}(\nabla \mathbf{v}_h)\|_\kappa\} \\
\leq& C_{\mathfrak{p},1} \max_{\kappa=K,K'}\{\|\sigma^{-1/2}\boldsymbol{\Pi}_{\mathbf{L^2}}(\nabla \mathbf{v}_h)\|_\kappa\}
\end{aligned}
$$

and then summing over all faces in the active mesh,

$$
\sum_{\substack{F\in\mathcal{F}^\sharp_{int} \\ F=\partial K\cap\partial K'}} \|\sigma^{-1/2}\{\!\{\boldsymbol{\Pi}_{\mathbf{L^2}}(\nabla \mathbf{v}_h)\}\!\}\cdot\mathbf{n}_F\|^2_F \leq C_{max}\|\nabla \mathbf{v}_h\|^2_{\Omega^\sharp}. \qquad (24)
$$

Likewise, using (15)

$$
\begin{aligned}
&\|\sigma^{-1/2}\mathbf{\Pi_{L^2}}(\nabla \mathbf{v}_h)\cdot \mathbf{n}_\Gamma\|_\Gamma^2\\
&=\sum_{K\cap\Gamma\neq\emptyset}\|\sigma^{-1/2}\mathbf{\Pi_{L^2}}(\nabla \mathbf{v}_h)\cdot \mathbf{n}_\Gamma\|_{K\cap\Gamma}^2\\
&\leq \sum_{K\cap\Gamma\neq\emptyset}\sigma^{-1/2}\sum_{i\in I_F^K} C_{INV}(\mathfrak{p},K,F_i^K)\frac{\mathfrak{p}^2|F_i|}{|K|}||\mathbf{\Pi_{L^2}}(\nabla \mathbf{v}_h)\cdot \mathbf{n}_\Gamma||_K^2\\
&\leq \sum_{K\cap\Gamma\neq\emptyset}\sigma^{-1/2}|I_F^K|\max_{i\in I_F^K}\{C_{INV}(\mathfrak{p},K,F_i^K)\}\frac{\mathfrak{p}^2|F_i|}{|K|}||\nabla \mathbf{v}_h||_K^2\\
&\leq C_{\mathfrak{p},2}\sum_{K\cap\Gamma\neq\emptyset}\|\nabla \mathbf{v}_h\|_K^2\leq C'_{max}\|\nabla \mathbf{v}_h\|_{\Omega^\sharp}^2. \qquad (25)
\end{aligned}
$$

Then, application of (16) verifies, for a suitable choice of λ, that the terms in (24) and (25) can be dominated by the leading two terms in (23). Indeed, letting C_{max} and C'_{max} the constants in (24) and (15) respectively and collecting all estimates, we conclude

$$
\begin{aligned}
\widetilde{a}_h(\mathbf{v}_h,\mathbf{v}_h)\geq&(C_u^{-1}-\lambda\sigma(C_{max}+C'_{max}))\|\nabla \mathbf{v}_h\|_{\Omega^\sharp}^2\\
&+(1-\lambda^{-1}\sigma^{-1})\big(\|\sigma^{1/2}\mathbf{v}_h\|_\Gamma^2+\sum_{F\in\mathcal{F}_{int}^\sharp}\|\sigma^{1/2}[\![\mathbf{v}_h]\!]\|_F^2\big).
\end{aligned}
$$

Coercivity (18) is already verified for $1>\lambda^{-1}\sigma^{-1}>C_u(C_{max}+C'_{max})$, or $1<\lambda\sigma<C_u(C_{max}+C'_{max})$ which is valid for $\lambda=(1+C_u(C_{max}+C'_max))/(2\sigma)$. The corresponding coercivity constant is $c_a=\min\{C_u^{-1}-\lambda\sigma(C_{max}+C'_{max}),1-\lambda^{-1}\sigma^{-1}\}$.

The proof of the continuity is standard and it is omitted for brevity. □

We recall also from [14, 20] the following lemma and corollary that will be used next.

Lemma 4.3. *Let $K\in\mathcal{T}^\sharp$ satisfy Assumptions 3.1 and 3.8, and let $\mathcal{K}\in\mathcal{T}^{cov}$ be the corresponding simplex with $K\subset\mathcal{K}$ as in Definition 3.7. Suppose that $v\in L^2(\Omega^\sharp)$ is such that the extension $\mathfrak{E}v|_{\mathcal{K}}\in H^{l_K}(\mathcal{K})$, for some $l_K\geq 0$, and that Assumption 3.8 is satisfied. Then, there exists an operator $\pi_{\mathfrak{p}}: H^{l_K}(\mathcal{K})\to\mathcal{P}^{\mathfrak{p}}(\mathcal{K})$, such that*

$$
||v-\pi_{\mathfrak{p}}v||_{H^q(K)}\leq C_1\frac{h_K^{s_K-q}}{\mathfrak{p}^{l_K-q}}||\mathfrak{E}v||_{H^{l_K}(\mathcal{K})}, \qquad (26)
$$

for $0\leq q\leq l_K$, and

$$
||v-\pi_{\mathfrak{p}}v||_{F_i}\leq \mathcal{C}_{ap}^{\frac{1}{2}}(\mathfrak{p},K,F_i)|F_i|^{\frac{1}{2}}\frac{h_K^{s_K-d/2}}{\mathfrak{p}^{l_K-1/2}}||\mathfrak{E}v||_{H^{l_K}(\mathcal{K})},\quad l_K\geq d/2, \qquad (27)
$$

with

$$
\mathcal{C}_{ap}(\mathfrak{p},K,F_i):=C_2\min\{\frac{h_K^d}{|F_i|\sup_{\mathbf{v}_{0,i}\in K}\min_{x\in F_i}(\mathbf{d}_i\cdot\mathbf{n})},\mathfrak{p}^{d-1}\},
$$

$s_K=\min\{\mathfrak{p}+1,l_K\}$, and C_1, $C_2>0$ constants depending only on the shape-regularity of $\mathcal{K}$, q, l_K, on C_{diam} (from Assumption 3.8) and on the domain $\Omega^\sharp$.

We note that the correspondence between $\mathcal{C}_{\rm INV}(\mathfrak{p},K,F_i)$ from Lemma 3.6, and $\mathcal{C}_{\rm ap}(\mathfrak{p},K,F_i)$ while $h_K^d\sim|K|$ is the typical case. The key attribute of both expressions is that they remain bounded for degenerating $|F_i|$, allowing for the estimates (13) and (27) to remain finite as $|F_i|\to 0$.

Corollary 4.4. *The approximation errors of the extended interpolation operators* $\boldsymbol{\pi}_{\mathfrak{p}}$ *and* $\pi_{\mathfrak{p}}$ *for* $(\mathbf{u},p)\in\left[H^{\mathfrak{p}+1}(\Omega^{\sharp})\right]^{d}\times H^{\mathfrak{p}}(\Omega^{\sharp})$ *satisfy*

$$|||\mathbf{u}-\boldsymbol{\pi}_{\mathfrak{p}}\mathbf{u}|||\leq C\sum_{K\in\mathcal{T}^{\sharp}}\frac{h_K^{\mathfrak{p}}}{\mathfrak{p}^{\mathfrak{p}-\frac{1}{2}}}\,||\mathbf{u}||_{\mathfrak{p}+1,\mathrm{K}}\,, \tag{28}$$

$$|||(\mathbf{u}-\boldsymbol{\pi}_{\mathfrak{p}}\mathbf{u},p-\pi_{\mathfrak{p}}p)|||\leq C\sum_{K\in\mathcal{T}^{\sharp}}\frac{h_K^{\mathfrak{p}}}{\mathfrak{p}^{\mathfrak{p}-\frac{1}{2}}}\Big(\,||\mathbf{u}||_{\mathfrak{p}+1,\mathrm{K}}+\frac{1}{\mathfrak{p}^{\frac{1}{2}}}\,||p||_{\mathfrak{p},\mathrm{K}}\Big). \tag{29}$$

Proof. It is convenient to introduce the auxiliary norm

$$\begin{aligned}|||\mathbf{v}|||_h^2=&\sum_{\mathcal{K}\in\mathcal{T}^{cov}}||\nabla v||_{\mathcal{K}}{}^2+\|\sigma^{1/2}\mathbf{v}\|_{\Gamma}^2+\sum_{F\in\mathcal{T}^{\sharp}\cap\Gamma}\|\mathfrak{p}^{-1}h_F^{1/2}\mathbf{n}_{\Gamma}\cdot\nabla\mathbf{v}\|_F^2\\&+\sum_{F\in\mathcal{F}_{int}^{\sharp}}\|\sigma^{1/2}[\![\mathbf{v}]\!]\|_F^2+\frac{1}{2}\sum_{K\in\mathcal{T}^{cov}}\|\mathfrak{p}^{-1}h_K^{1/2}\nabla\mathbf{v}|_K\cdot\mathbf{n}_{\partial K}\|_{\partial K}^2,\end{aligned}$$

see also [14, p.60]. This norm clearly bounds $|||\mathbf{v}|||$, in the sense that $|||\mathbf{v}-\boldsymbol{\pi}_{\mathfrak{p}}\mathbf{v}|||\leq\left|\left|\left|\mathfrak{E}^{\mathfrak{p}+1}\mathbf{v}-\boldsymbol{\pi}_{\mathfrak{p}}\mathbf{v}\right|\right|\right|_h$. Hence, we may prove the estimate for $|||\cdot|||_h$ instead of $|||\cdot|||$. Setting $\mathbf{e}_{\pi}=\mathfrak{E}^{\mathfrak{p}+1}\mathbf{u}-\boldsymbol{\pi}_{\mathfrak{p}}\mathbf{u}$, we take by definition

$$\begin{aligned}|||\mathbf{e}_{\pi}|||_h^2=&\sum_{\mathcal{K}\in\mathcal{T}^{cov}}||\nabla\mathbf{e}_{\pi}||_{\mathcal{K}}{}^2+\|\sigma^{1/2}\mathbf{e}_{\pi}\|_{\Gamma}^2+\sum_{F\in\mathcal{T}^{\sharp}\cap\Gamma}\|\mathfrak{p}^{-1}h_F^{1/2}\nabla\mathbf{e}_{\pi}\cdot\mathbf{n}_F\|_F^2\\&+\sum_{F\in\mathcal{F}_{int}^{\sharp}}\|\sigma^{1/2}[\![\mathbf{e}_{\pi}]\!]\|_F^2+\sum_{F\in\mathcal{F}_{int}^{\sharp}}\|\mathfrak{p}^{-1}h_F^{1/2}\{\!\{\nabla\mathbf{e}_{\pi}\}\!\}\cdot\mathbf{n}_F\|_F^2.\end{aligned}$$

All the above terms may be estimated, using the local approximation properties (26)–(27), the aforementioned inverse estimates and the stability of the extension operator $\mathfrak{E}^{k+1}$. For instance,

$$\sum_{\mathcal{K}\in\mathcal{T}^{cov}}\|\nabla\mathbf{e}_{\pi}\|_{\mathcal{K}}\leq\sum_{\mathcal{K}\in\mathcal{T}^{cov}}\|\mathbf{e}_{\pi}\|_{H^1(\mathcal{K})}\overset{(26)}{\leq}C\sum_{\mathcal{K}\in\mathcal{T}^{cov}}\frac{h_{\mathcal{K}}^{\mathfrak{p}}}{\mathfrak{p}^{\mathfrak{p}}}||\mathfrak{E}u||_{H^{\mathfrak{p}+1}(\mathcal{K})},$$

after choosing $q=1$, $l_k=\mathfrak{p}+1$ and $s^k=\min(\mathfrak{p}+1,l_k)$ in (26). Similarly, we derive

$$\begin{aligned}\sum_{F\in\mathcal{T}^{\sharp}\cap\Gamma}\|\mathfrak{p}h_F^{-1/2}\mathbf{e}_{\pi}\|_F\overset{(27)}{\leq}&C\sum_{\mathcal{K}\in\mathcal{T}^{cov}}\mathfrak{p}h_{\mathcal{K}}^{-1/2}\frac{h_{\mathcal{K}}^{\mathfrak{p}+1/2}}{\mathfrak{p}^{\mathfrak{p}+1/2}}||\mathfrak{E}u||_{H^{\mathfrak{p}+1}(\mathcal{K})}\\=&C\sum_{\mathcal{K}\in\mathcal{T}^{cov}}\frac{h_{\mathcal{K}}^{\mathfrak{p}}}{\mathfrak{p}^{\mathfrak{p}-\frac{1}{2}}}||\mathfrak{E}u||_{H^{\mathfrak{p}+1}(\mathcal{K})},\end{aligned}$$

e.g. for $d=2$, $l_k=\mathfrak{p}+1$. Let $F\subset\partial K$. As we have seen in the variational formulation, the norm $||\nabla e_p\cdot\mathbf{n}_F||_F$ can be efficiently approximated by $||\nabla e_p\cdot\mathbf{n}_F||_F\leq C\frac{\mathfrak{p}}{h_K^{1/2}}||\nabla e_p||_{L^2(K)}$. We note that inserting the Π_{L^2} projection we are losing $\mathfrak{p}^{1/2}$ accuracy, [27], although this is consistent with the half power we lose from the penalization of the method and we can prove optimal a–priori error bounds. Finally, we take

$$\begin{aligned}\sum_{F\in\mathcal{T}^{\sharp}\cap\Gamma}||\mathfrak{p}^{-1}h_F^{1/2}\cdot\nabla e_p\cdot\mathbf{n}_F||_F\leq&C\sum_{\mathcal{K}\in\mathcal{T}^{cov}}\mathfrak{p}^{-1}h_{\mathcal{K}}^{1/2}\frac{\mathfrak{p}}{h_{\mathcal{K}}^{1/2}}||\nabla e_p||_{\mathcal{K}}\\\leq&C\sum_{\mathcal{K}\in\mathcal{T}^{cov}}\frac{h_{\mathcal{K}}^{\mathfrak{p}}}{\mathfrak{p}^{\mathfrak{p}}}||\mathfrak{E}u||_{H^{\mathfrak{p}+1}(\mathcal{K})}.\end{aligned}$$

Proceeding in a similar fashion, we have

$$\sum_{F\in\mathcal{F}_{int}^{\sharp}}\|\sigma[\![\mathbf{e}_\pi]\!]\|_F=\sum_{F\in\mathcal{F}_{int}^{\sharp}}\|\mathfrak{p}h_F^{-1/2}[\![\mathbf{e}_\pi]\!]\|_F\leq C\sum_{\mathcal{K}\in\mathcal{T}^{cov}}\frac{h_{\mathcal{K}}^{\mathfrak{p}}}{\mathfrak{p}^{\mathfrak{p}-\frac{1}{2}}}||\mathfrak{E}u||_{H^{\mathfrak{p}+1}(\mathcal{K})},$$

$$\sum_{F\in\mathcal{F}_{int}^{\sharp}}\|\mathfrak{p}^{-1}h_F^{1/2}\{\!\{\nabla\mathbf{e}_\pi\}\!\}\cdot\mathbf{n}_F\|_F^2\leq C\sum_{\mathcal{K}\in\mathcal{T}^{cov}}\frac{h_{\mathcal{K}}^{\mathfrak{p}}}{\mathfrak{p}^{\mathfrak{p}}}||\mathfrak{E}u||_{H^{\mathfrak{p}+1}(\mathcal{K})},$$

and the proof of (29) is complete. The proof of the estimate (29) for the approximation error in the product space is similar, considering the auxiliary pressure norm

$$|||p|||_h^2=\sum_{\mathcal{K}\in\mathcal{T}^{cov}}\|p\|_{\mathcal{K}}^2+\sum_{F\in\mathcal{T}^{\sharp}\cap\Gamma}\|\mathfrak{p}^{-1}h_F^{1/2}p\|_F^2+\sum_{F\in\mathcal{F}_{int}^{\sharp}}\|\mathfrak{p}^{-1}h_F^{1/2}[\![p]\!]\|_F^2$$

and proving the assertion for $e_\pi=|||\mathfrak{E}p-\pi_{\mathfrak{p}}p|||_h$. In particular we can employ a multiplicative trace inequality:

$$||q||_{\partial K}^2\leq C(||q||_K||\nabla q||_K+h_K^{-1}||q||_K^2),\quad q\in H^1(K),$$

[30, p2140], [55, p1571], and we conclude to

$$\begin{aligned}
&\sum_{F\in\mathcal{T}^{\sharp}}\|\mathfrak{p}^{-1}h_F^{1/2}e_\pi\|_F^2\\
\leq& C\sum_{K\in\mathcal{T}^{\sharp}}\big(||\mathfrak{p}^{-1}h_K^{1/2}e_\pi||_K||\mathfrak{p}^{-1}h_K^{1/2}\nabla e_\pi||_K+h_K^{-1}||\mathfrak{p}^{-1}h_K^{1/2}e_\pi||_K^2\big)\\
\overset{q=0,s_K=l_K=\mathfrak{p}}{\leq}& C\sum_{\substack{\mathcal{K}\in\mathcal{T}^{cov}\\K\in\mathcal{T}^{\sharp}}}\big(\frac{h_K^{s_K-0}}{\mathfrak{p}^{\mathfrak{p}-0}}||\mathfrak{p}^{-1}h_K^{1/2}\mathfrak{E}p||_{H^{\mathfrak{p}}(\mathcal{K})}||\mathfrak{p}^{-1}h_K^{1/2}\nabla e_\pi||_K+h_K^{-1}||\mathfrak{p}^{-1}h_K^{1/2}e_\pi||_K^2\big)\\
\leq& C\sum_{\substack{\mathcal{K}\in\mathcal{T}^{cov}\\K\in\mathcal{T}^{\sharp}}}\big(\frac{h_K^{\mathfrak{p}}}{\mathfrak{p}^{\mathfrak{p}}}||\mathfrak{p}^{-1}h_K{}^{1/2}\mathfrak{E}p||_{H^{\mathfrak{p}}(\mathcal{K})}\frac{\mathfrak{p}^2}{h_K}||\mathfrak{p}^{-1}h_K^{1/2}e_\pi||_K+h_K^{-1}||\mathfrak{p}^{-1}h_K^{1/2}e_\pi||_K^2\big)\\
\leq& C\sum_{\substack{\mathcal{K}\in\mathcal{T}^{cov}\\K\in\mathcal{T}^{\sharp}}}\big(\frac{h_K^{\mathfrak{p}}}{\mathfrak{p}^{\mathfrak{p}}}||\mathfrak{p}^{-1}h_K^{1/2}\mathfrak{E}p||_{H^{\mathfrak{p}}(\mathcal{K})}\frac{\mathfrak{p}}{h_K^{1/2}}||e_\pi||_K+\mathfrak{p}^{-2}||e_\pi||_K^2\big),
\end{aligned}$$

and finally with standard algebra

$$\begin{aligned}
\sum_{F\in\mathcal{T}^{\sharp}}\|\mathfrak{p}^{-1}h_F^{1/2}e_\pi\|_F^2\leq& C\sum_{\substack{\mathcal{K}\in\mathcal{T}^{cov}\\K\in\mathcal{T}^{\sharp}}}\big(\frac{h_K^{\mathfrak{p}}}{\mathfrak{p}^{\mathfrak{p}}}||\mathfrak{E}p||_{H^{\mathfrak{p}}(\mathcal{K})}||e_\pi||_K+\mathfrak{p}^{-2}||e_\pi||_K^2\big)\\
\leq& C\sum_{\mathcal{K}\in\mathcal{T}^{cov}}\big(\frac{h_K^{\mathfrak{p}}}{\mathfrak{p}^{\mathfrak{p}}}||\mathfrak{E}p||_{H^{\mathfrak{p}}(\mathcal{K})}\frac{h_K^{\mathfrak{p}}}{\mathfrak{p}^{\mathfrak{p}}}||\mathfrak{E}p||_{H^{\mathfrak{p}}(\mathcal{K})}+\mathfrak{p}^{-2}\frac{h_K^{2\mathfrak{p}}}{\mathfrak{p}^{2\mathfrak{p}}}||\mathfrak{E}p||_{H^{\mathfrak{p}}(\mathcal{K})}^2\big)\\
\leq& C\sum_{\mathcal{K}\in\mathcal{T}^{cov}}\big(\frac{h_K^{2\mathfrak{p}}}{\mathfrak{p}^{2\mathfrak{p}}}||\mathfrak{E}p||_{H^{\mathfrak{p}}(\mathcal{K})}^2+\frac{h_K^{2\mathfrak{p}}}{\mathfrak{p}^{2(\mathfrak{p}+1)}}||\mathfrak{E}p||_{H^{\mathfrak{p}}(\mathcal{K})}^2\big)\\
\leq& C\sum_{\mathcal{K}\in\mathcal{T}^{cov}}\frac{h_K^{2\mathfrak{p}}}{\mathfrak{p}^{2\mathfrak{p}}}||\mathfrak{E}p||_{H^{\mathfrak{p}}(\mathcal{K})}^2,
\end{aligned}$$

which completes the proof. □

We continue with the stability for the b_h proof.

Lemma 4.5. *There exists $C > 0$, such that for every $p_h \in Q_h^\sharp$ we have*

$$C \left\| p_h \right\|_{\Omega^\sharp} \leq \sup_{\mathbf{w}_h \in V_h^\sharp \setminus \{0\}} \frac{b_h(\mathbf{w}_h, p_h)}{\left|\!\left|\!\left| \mathbf{w}_h \right|\!\right|\!\right|_{V^c}} + \Big(\sum_{K \in \mathcal{T}^\sharp} \left\| \mathfrak{p}^{-2} h_K \nabla p_h \right\|_K^2 \Big)^{1/2}$$
$$+ \Big(\sum_{F \in \mathcal{F}_{int}^\sharp} \left\| \mathfrak{p}^{-1} h_F^{1/2} [\![p_h]\!] \right\|_F^2 \Big)^{1/2}. \tag{30}$$

Proof. Considering a fixed $p_h \in Q_h^\sharp$, due to the surjectivity of the divergence operator there exists a $\mathbf{v}_{p_h} \in \left[H_0^1(\Omega^\sharp) \right]^d$, such that

$$\nabla \cdot \mathbf{v}_{p_h} = p_h \quad \text{(a)} \quad \text{and} \quad C_{\Omega^\sharp} \left\| \mathbf{v}_{p_h} \right\|_{1,\Omega^\sharp} \leq \left\| p_h \right\|_{\Omega^\sharp} \quad \text{(b)} \tag{31}$$

for some constant $C_{\Omega^\sharp} > 0$. Then, applying integration by parts on each element and the fact that $\mathbf{v}_{p_h}$ and $[\![\mathbf{v}_{p_h}]\!]$ vanish on Γ and on $F \in \mathcal{F}_{int}^\sharp$ respectively –since $\mathbf{v}_{p_h} \in \left[H_0^1(\Omega^\sharp) \right]^d$ is an element of the continuous space– implies

$$\begin{aligned}
\left\| p_h \right\|_{\Omega^\sharp}^2 &= \int_{\Omega^\sharp} p_h \left(\nabla \cdot \mathbf{v}_{p_h} \right) d\boldsymbol{x} \\
&= - \int_{\Omega^\sharp} \mathbf{v}_{p_h} \nabla p_h \, d\boldsymbol{x} + \sum_{K \in \mathcal{T}^\sharp} \int_{\partial K} \left(\mathbf{v}_{p_h} \cdot \mathbf{n}_F \right) p_h \, d\boldsymbol{x} \\
&= - \int_{\Omega^\sharp} \mathbf{v}_{p_h} \nabla p_h \, d\boldsymbol{x} + \sum_{F \in \mathcal{F}_{int}^\sharp} \int_F \{\!\!\{ \mathbf{v}_{p_h} \}\!\!\} \cdot \mathbf{n}_F [\![p_h]\!] \, d\gamma \\
&\quad + \sum_{F \in \mathcal{F}_{int}^\sharp} \int_F [\![\mathbf{v}_{p_h}]\!] \cdot \mathbf{n}_F \{\!\!\{ p_h \}\!\!\} \, d\gamma + \int_{\Gamma \cap K} \left(\mathbf{v}_{p_h} \cdot \mathbf{n}_\Gamma \right) p_h \, d\gamma \\
&= - \int_{\Omega^\sharp} \mathbf{v}_{p_h} \nabla p_h \, d\boldsymbol{x} + \sum_{F \in \mathcal{F}_{int}^\sharp} \int_F \{\!\!\{ \mathbf{v}_{p_h} \}\!\!\} \cdot \mathbf{n}_F [\![p_h]\!] \, d\gamma.
\end{aligned}$$

Next, we introduce interpolation error $\mathbf{e}_h := \boldsymbol{\pi}_\mathfrak{p} \mathbf{v}_{p_h} - \mathbf{v}_{p_h}$ for $\mathbf{v}_{p_h} \mapsto \boldsymbol{\pi}_\mathfrak{p} \mathbf{v}_{p_h} \in V_h^\sharp$ in the previous expression and holds that

$$\begin{aligned}
\left\| p_h \right\|_{\Omega^\sharp}^2 &= \int_{\Omega^\sharp} \mathbf{e}_h \nabla p_h \, d\boldsymbol{x} - \int_{\Omega^\sharp} \boldsymbol{\pi}_\mathfrak{p} \mathbf{v}_{p_h} \nabla p_h \, d\boldsymbol{x} + \sum_{F \in \mathcal{F}_{int}^\sharp} \int_F \{\!\!\{ \mathbf{v}_{p_h} \}\!\!\} \cdot \mathbf{n}_F [\![p_h]\!] \, d\gamma \\
&\overset{(5)}{=} \int_{\Omega^\sharp} \mathbf{e}_h \nabla p_h \, d\boldsymbol{x} - b_h(\pi_\mathfrak{p} \mathbf{v}_{p_h}, p_h) - \sum_{F \in \mathcal{F}_{int}^\sharp} \int_F \{\!\!\{ \mathbf{e}_h \}\!\!\} \cdot \mathbf{n}_F [\![p_h]\!] \, d\gamma.
\end{aligned} \tag{32}$$

For the first term, the Cauchy–Schwarz inequality, (26) and (31)a, yields

$$\begin{aligned}
\Big| \int_{\Omega^\sharp} \mathbf{e}_h \nabla p_h \, d\boldsymbol{x} \Big| &\leq \Big(\sum_{K \in \mathcal{T}^\sharp} \left\| \mathfrak{p} h_K^{-1/2} \mathbf{e}_h \right\|_K^2 \Big)^{1/2} \Big(\sum_{K \in \mathcal{T}^\sharp} \left\| \mathfrak{p}^{-1} h_K^{1/2} \nabla p_h \right\|_K^2 \Big)^{1/2} \\
&\overset{(26)}{\leq} C \left\| \mathbf{v}_{p_h} \right\|_{1,\Omega^\sharp} \Big(\sum_{K \in \mathcal{T}^\sharp} \left\| \mathfrak{p}^{-1} {h_K}^{1/2} \nabla p_h \right\|_K^2 \Big)^{1/2} \\
&\overset{(31)a}{\leq} C C_{\Omega^\sharp}^{-1} \left\| p_h \right\|_{\Omega^\sharp} \Big(\sum_{K \in \mathcal{T}^\sharp} \left\| \mathfrak{p}^{-1} h_K^{1/2} \nabla p_h \right\|_K^2 \Big)^{1/2}.
\end{aligned} \tag{33}$$

Employing the continuity property of the extended interpolation operator and (31),

$$
\begin{aligned}
|b_h(\boldsymbol{\pi}_{\mathfrak{p}}\mathbf{v}_{p_h},p_h)| =& \frac{|b_h(\boldsymbol{\pi}_{\mathfrak{p}}\mathbf{v}_{p_h},p_h)|}{|||\boldsymbol{\pi}_{\mathfrak{p}}\mathbf{v}_{p_h}|||_{V^c}}|||\boldsymbol{\pi}_{\mathfrak{p}}\mathbf{v}_{p_h}|||_{V^c}\\
\leq& \Big(\sup_{\mathbf{w}_h\in V_h^\sharp\setminus\{0\}}\frac{b_h(\mathbf{w}_h,p_h)}{|||\mathbf{w}_h|||_{V^c}}\Big)C_{proj}\,\|\mathbf{v}_{p_h}\|_{1,\Omega^\sharp}\\
\leq& \Big(\sup_{\mathbf{w}_h\in V_h^\sharp\setminus\{0\}}\frac{b_h(\mathbf{w}_h,p_h)}{|||\mathbf{w}_h|||_{V^c}}\Big)C_{proj}C_{\Omega^\sharp}^{-1}\,\|p_h\|_{\Omega^\sharp}\,. \qquad (34)
\end{aligned}
$$

To handle the third term, we follow the steps similarly as we did for the first term using (27) and we conclude to

$$
\begin{aligned}
&\Big|\sum_{F\in\mathcal{F}_{int}^\sharp}\int_F\{\!\{\mathbf{e}_h\}\!\}\cdot\mathbf{n}_F[\![p_h]\!]\,d\gamma\Big|\\
\leq&\Big(\sum_{F\in\mathcal{F}_{int}^\sharp}\big\|\mathfrak{p}h_F^{-1/2}\{\!\{\mathbf{e}_h\}\!\}\big\|_F^2\Big)^{1/2}\Big(\sum_{F\in\mathcal{F}_{int}^\sharp}\big\|\mathfrak{p}^{-1}h_F^{1/2}[\![p_h]\!]\big\|_F^2\Big)^{1/2}\\
\leq& C\big\|\mathbf{v}_{p_h}\big\|_{1,\Omega^\sharp}\Big(\sum_{F\in\mathcal{F}_{int}^\sharp}\big\|\mathfrak{p}^{-1}h_F^{1/2}[\![p_h]\!]\big\|_F^2\Big)^{1/2}\\
\leq& CC_{\Omega^\sharp}^{-1}\,\|p_h\|_{\Omega^\sharp}\Big(\sum_{F\in\mathcal{F}_{int}^\sharp}\big\|\mathfrak{p}^{-1}h_F^{1/2}[\![p_h]\!]\big\|_F^2\Big)^{1/2}. \qquad (35)
\end{aligned}
$$

Finally, we collect the inequalities (33)-(35), and the proof is completed. □

An instant conclusion is the following.

Corollary 4.6. *For every $p_h\in Q_h^\sharp$, there exists $\mathbf{w}_h\in V_h^\sharp$, such that*

$$
\begin{aligned}
b_h(\mathbf{w}_h,-p_h)\geq\|p_h\|_{\Omega^\sharp}^2 - C_\sigma\Big(&\big(\sum_{K\in\mathcal{T}^\sharp}\big\|\mathfrak{p}^{-2}h_K\nabla p_h\big\|_K^2\big)^{1/2}\\
&+\big(\sum_{F\in\mathcal{F}_{int}^\sharp}\big\|\mathfrak{p}^{-1}{h_F}^{1/2}[\![p_h]\!]\big\|_F^2\big)^{1/2}\Big)\,\|p_h\|_{\Omega^\sharp}\,, \qquad (36)
\end{aligned}
$$

for suitable $C_\sigma>0$.

Proof. We denote by C_1, C_2 the constants appearing in (33), (35), we rearrange (32) and we derive

$$
b_h(\boldsymbol{\pi}_{\mathfrak{p}}\mathbf{v}_{p_h},-p_h)\geq\|p_h\|_{\Omega^\sharp}^2-\Big|\int_{\Omega^\sharp}\mathbf{e}_h\nabla p_h\,d\boldsymbol{x}\Big|-\Big|\sum_{F\in\mathcal{F}_{int}^\sharp}\int_F\{\!\{\mathbf{e}_h\}\!\}\cdot\mathbf{n}_F[\![p_h]\!]\,d\gamma\Big|,
$$

hence, the result clearly follows for $\mathbf{w}_h=\boldsymbol{\pi}_{\mathfrak{p}}\mathbf{v}_{p_h}$ with $C_\sigma=\max\{C_1,C_2\}$. □

Next, we pass to the discrete inf–sup stability which is being proven below.

Theorem 4.7. *There is a constant $c_{bil}>0$, such that for all $(\mathbf{u}_h,p_h)\in V_h^\sharp\times Q_h^\sharp$, we have*

$$
c_{bil}|||(\mathbf{u}_h,p_h)|||_{V^c,Q^c}\leq\sup_{(\mathbf{v}_h,q_h)\in V_h^\sharp\times Q_h^\sharp}\frac{A_h(\mathbf{u}_h,p_h;\mathbf{v}_h,q_h)}{|||(\mathbf{v}_h,q_h)|||_{V^c,Q^c}}. \qquad (37)
$$

Proof. Similar to [2], let $(\mathbf{u}_h, p_h) \in V_h^\sharp \times Q_h^\sharp$ and note by Corollary 4.6 that there exists $\mathbf{w}_h \in V_h^\sharp$ in (36). As a matter of fact, there is no loss of generality in setting $|||\mathbf{w}_h|||_{V^c} = \|p_h\|_{\Omega^\sharp}$ and then inequality (36) combined with the Young inequality and factorizing with respect to $\|p_h\|_{\Omega^\sharp}^2$ we obtain

$$\begin{aligned} b_h(\mathbf{w}_h, -p_h) \geq & \big(1 - \frac{C_\sigma \lambda}{2}\big) \|p_h\|_{\Omega^\sharp}^2 - \frac{C_\sigma}{2\lambda}\Big(\big(\sum_{K \in \mathcal{T}^\sharp} \big\|\mathfrak{p}^{-2} h_K \nabla p_h\big\|_K^2 \big)^{1/2} \\ & + \big(\sum_{F \in \mathcal{F}_{int}^\sharp} \big\|\mathfrak{p}^{-1} h_F^{1/2} [\![p_h]\!]\big\|_F^2 \big)^{1/2} \Big)^2 \\ \geq & \big(1 - \frac{C_\sigma \lambda}{2}\big) \|p_h\|_{\Omega^\sharp}^2 - \frac{C_\sigma}{\lambda} \sum_{K \in \mathcal{T}^\sharp} \big\|\mathfrak{p}^{-2} h_K \nabla p_h\big\|_K^2 \\ & - \frac{C_\sigma}{\lambda} \sum_{F \in \mathcal{F}_{int}^\sharp} \big\|\mathfrak{p}^{-1} h_F^{1/2} [\![p_h]\!]\big\|_F^2. \end{aligned} \tag{38}$$

We focus now on showing that for a sensible choice of parameters $\zeta_1 > 0$ and $\zeta_2 > 0$, there exists a constant $c_{bil} > 0$ such that the test pair $(\mathbf{v}_h, q_h) = (\mathbf{u}_h, -p_h) + \zeta_1(-\mathbf{w}_h, 0) + \zeta_2(-\mathfrak{p}^{-4}\theta \nabla p_h, 0)$, for proper $\theta \in \mathbb{R}$ that will be chosen later, yields

$$A_h(\mathbf{u}_h, p_h; \mathbf{v}_h, q_h) \geq c_{bil} |||(\mathbf{u}_h, p_h)|||_{V^c, Q^c} |||(\mathbf{v}_h, q_h)|||_{V^c, Q^c}, \tag{39}$$

whereby the desired outcome (37) is then provided.

Consequently, if we initially test with $(\mathbf{u}_h, -p_h)$ using the coercivity estimate (18) of $\widetilde{a}_h$, we derive

$$A_h(\mathbf{u}_h, p_h; \mathbf{u}_h, -p_h) = \widetilde{a}_h(\mathbf{u}_h, \mathbf{u}_h) \geq c_a |||\mathbf{u}_h|||_{V^c}^2. \tag{40}$$

Thus, we consider $(-\mathbf{w}_h, 0)$ in (38) and utilize the continuity estimate (19) of $\widetilde{a}_h$ together with the Young inequality,

$$\begin{aligned} A_h(\mathbf{u}_h, p_h; -\mathbf{w}_h, 0) = & - \widetilde{a}_h(\mathbf{u}_h, \mathbf{w}_h) + b_h(\mathbf{w}_h, -p_h) \\ \geq & - \frac{C_a}{2\lambda} |||\mathbf{u}_h|||_{V^c}^2 + \big(1 - \frac{C_a \lambda}{2} - \frac{C_\sigma \lambda}{2}\big) \|p_h\|_{\Omega^\sharp}^2 \\ & - \frac{C_\sigma}{\lambda} \sum_{K \in \mathcal{T}^\sharp} \big\|\mathfrak{p}^{-2} h_K \nabla p_h\big\|_K^2 - \frac{C_\sigma}{\lambda} \sum_{F \in \mathcal{F}_{int}^\sharp} \big\|\mathfrak{p}^{-1} {h_F}^{1/2} [\![p_h]\!]\big\|_F^2 \\ \geq & - C_1 |||\mathbf{u}_h|||_{V^c}^2 + C_2 \|p_h\|_{\Omega^\sharp}^2 - C_3 \sum_{K \in \mathcal{T}^\sharp} \big\|\mathfrak{p}^{-2} h_K \nabla p_h\big\|_K^2 \\ & - C_3 \sum_{F \in \mathcal{F}_{int}^\sharp} \big\|\mathfrak{p}^{-1} {h_F}^{1/2} [\![p_h]\!]\big\|_F^2, \end{aligned} \tag{41}$$

where $C_1 = \frac{C_a}{2\lambda}$, $C_2 = 1 - \frac{C_a + C_\sigma}{2}\lambda$ and $C_3 = \frac{C_\sigma}{\lambda}$ are positive constants for small enough $0 < \lambda < \frac{2}{C_a + C_\sigma}$. Therefore, to gain the desired control and to balance the negative contribution $\|\mathfrak{p}^{-4} h_K^2 \nabla p_h\|_K^2$ in (41), we test with $(-\mathfrak{p}^{-4}\theta \nabla p_h, 0)$ using the continuity estimate (19) for $\widetilde{a}_h$, the Cauchy-Schwarz inequality, the inverse estimate

(11) and Young inequality. In particular,

$$
\begin{aligned}
&A_h(\mathbf{u}_h, p_h; -\mathfrak{p}^{-4}\theta\nabla p_h, 0)\\
=&\widetilde{a}_h(\mathbf{u}_h, -\mathfrak{p}^{-4}\theta\nabla p_h) + b_h(-\mathfrak{p}^{-4}\theta\nabla p_h, p_h)\\
\geq& -|\widetilde{a}_h(\mathbf{u}_h, -\mathfrak{p}^{-4}\theta\nabla p_h)| - \sum_{K\in\mathcal{T}^\sharp}\left\|\mathfrak{p}^{-2}\theta^{1/2}\nabla p_h\right\|_K^2\\
&+\sum_{F\in\mathcal{F}^\sharp_{int}}\int_F \{\!\{\mathfrak{p}^{-4}\theta\nabla p_h\}\!\}\cdot\mathbf{n}_F[\![p_h]\!]\,d\gamma\\
\geq& -C_a|\!|\!|\mathbf{u}_h|\!|\!|_{V^c}|\!|\!|\mathfrak{p}^{-4}\theta\nabla p_h|\!|\!|_{V^c} - \sum_{K\in\mathcal{T}^\sharp}\left\|\mathfrak{p}^{-2}\theta^{1/2}\nabla p_h\right\|_K^2\\
&+\widehat{C}\Big(\sum_{F\in\mathcal{F}^\sharp_{int}}\|\mathfrak{p}^{-3}\theta^{3/4}\nabla p_h\cdot\mathbf{n}_F\|_F^2\Big)^{1/2}\Big(\sum_{F\in\mathcal{F}^\sharp_{int}}\|\mathfrak{p}^{-1}\theta^{1/4}[\![p_h]\!]\|_F^2\Big)^{1/2}
\end{aligned}
$$

and we conclude to

$$
\begin{aligned}
&A_h(\mathbf{u}_h, p_h; -\mathfrak{p}^{-4}\theta\nabla p_h, 0)\\
\geq& -\frac{C_a}{2\lambda_1}|\!|\!|\mathbf{u}_h|\!|\!|_{V^c}^2 - \frac{C_a\lambda_1}{2}|\!|\!|\mathfrak{p}^{-4}\theta\nabla p_h|\!|\!|_{V^c}^2 - \sum_{K\in\mathcal{T}^\sharp}\left\|\mathfrak{p}^{-2}\theta^{1/2}\nabla p_h\right\|_K^2\\
&+C\Big(\sum_{K\in\mathcal{T}^\sharp}\|\mathfrak{p}^{-2}\theta^{3/4}h_K^{-1/2}\nabla p_h\|_K^2\Big)^{1/2}\Big(\sum_{F\in\mathcal{F}^\sharp_{int}}\|\mathfrak{p}^{-1}\theta^{1/4}[\![p_h]\!]\|_F^2\Big)^{1/2}\\
\overset{(43),\,\theta=h_K^2}{\geq}& -\frac{C_a}{2\lambda_1}|\!|\!|\mathbf{u}_h|\!|\!|_{V^c}^2 - \frac{\widetilde{C}C_a\lambda_1}{2}\sum_{\mathcal{K}\in\mathcal{T}^{cov}}\left\|\mathfrak{p}^{-2}h_K\nabla p_h\right\|_{\mathcal{K}}^2 - \sum_{K\in\mathcal{T}^\sharp}\left\|\mathfrak{p}^{-2}h_K\nabla p_h\right\|_K^2\\
&+\frac{C\lambda_2}{2}\sum_{K\in\mathcal{T}^\sharp}\left\|\mathfrak{p}^{-2}h_K\nabla p_h\right\|_K^2 + \frac{C}{2\lambda_2}\sum_{F\in\mathcal{F}^\sharp_{int}}\left\|\mathfrak{p}^{-1}h_F^{1/2}[\![p_h]\!]\right\|_F^2\\
\geq& -\frac{C_a}{2\lambda_1}|\!|\!|\mathbf{u}_h|\!|\!|_{V^c}^2 - \sum_{K\in\mathcal{T}^\sharp}\left\|\mathfrak{p}^{-2}h_K\nabla p_h\right\|_K^2 - \frac{C_p}{2}(\widetilde{C}C_a\lambda_1\\
&-C\lambda_2)\left\|\mathfrak{p}^{-2}h_K\nabla p_h\right\|_{\Omega^\sharp}^2 + \frac{C}{2\lambda_2}\sum_{F\in\mathcal{F}^\sharp_{int}}\left\|\mathfrak{p}^{-1}h_F^{1/2}[\![p_h]\!]\right\|_F^2\\
\geq& -C_4|\!|\!|\mathbf{u}_h|\!|\!|_{V^c}^2 + C_5\sum_{K\in\mathcal{T}^\sharp}\left\|\mathfrak{p}^{-2}h_K\nabla p_h\right\|_K^2 + C_6\sum_{F\in\mathcal{F}^\sharp_{int}}\left\|\mathfrak{p}^{-1}h_F^{1/2}[\![p_h]\!]\right\|_F^2 \qquad (42)
\end{aligned}
$$

where $C_4 = \frac{C_a}{2\lambda_1}$, $C_5 = 1 - \frac{c_p}{2}(\widetilde{C}C_a\lambda_1 - C\lambda_2)$ and $C_6 = \frac{C}{2\lambda_2}$ are positive constants for properly chosen

$$\lambda_1 > 2/(c_p\widetilde{C}C_a) > 0$$

and

$$0 < \lambda_2 < 2/(c_pC)(c_p\widetilde{C}C_a\lambda_1/2 - 1).$$

We note that in the last inequality $\widetilde{C} > 0$, we take $\sigma = \mathfrak{p} h_K^{-1/2}$ and we derive the bound

$$
\begin{aligned}
&\left|\left|\left|\mathfrak{p}^{-4}\theta\nabla p_h\right|\right|\right|_{V^c}^2 \\
&= \left\|\mathfrak{p}^{-4}\theta\nabla\nabla p_h\right\|_{\Omega^{\mathrm{cov}}}^2 + \sum_{F\in\mathcal{T}^\sharp\cap\Gamma}\left\|\mathfrak{p}^{-3}\theta h_F^{-1/2}\nabla p_h\right\|_F^2 + \sum_{F\in\mathcal{F}_{int}^\sharp}\left\|\mathfrak{p}^{-3}\theta h_F^{-1/2}[\![\nabla p_h]\!]\right\|_F^2 \\
&\leq \sum_{\mathcal{K}\in\mathcal{T}^{cov}}\left\|\mathfrak{p}^{-2}\theta h_K^{-1}\nabla p_h\right\|_{\mathcal{K}}^2 + \sum_{F\in\mathcal{T}^\sharp\cap\Gamma}\left\|\mathfrak{p}^{-3}\theta h_F^{-1/2}\nabla p_h\right\|_F^2 + \sum_{F\in\mathcal{F}_{int}^\sharp}\left\|\mathfrak{p}^{-3}\theta h_F^{-1/2}[\![\nabla p_h]\!]\right\|_F^2 \\
&\leq \widetilde{C}\sum_{\mathcal{K}\in\mathcal{T}^{cov}}\left\|\mathfrak{p}^{-2}h_K\nabla p_h\right\|_{\mathcal{K}}^2
\end{aligned}
\tag{43}
$$

which has been obtained by the trace inequalities (11), the inverse inequality (14) and finally setting $\theta = h_K^2$. In particular, if we regard the norm on a facet $F \subset \partial K \in \mathcal{T}^\sharp$,

$$
\left\|\sigma\mathfrak{p}^{-4}h_F^2\nabla p_h\right\|_F \leq \left\|\mathfrak{p}^{-3}h_F^{3/2}\nabla p_h\right\|_F \leq \left\|\mathfrak{p}^{-3}h_F^{3/2}\nabla p_h\right\|_{\partial K} \leq C\mathfrak{p}^{-2}h_K\left\|\nabla p_h\right\|_K,
$$

by (11) and (14) respectively. Then, the norm corresponding to the jump on $F = K \cap K'$ satisfies $\left\|\mathfrak{p}^{-3}h_F^{3/2}[\![\nabla p_h]\!]\right\|_F \leq C\mathfrak{p}^{-2}h_K \max\left\{\left\|[\nabla p_h\right\|_K, \left\|[\nabla p_h\right\|_{K'}\right\}$ leading to the estimate

$$
\sum_{F\in\mathcal{F}_{int}^\sharp}\left\|\mathfrak{p}^{-3}h_F^{3/2}[\![\nabla p_h]\!]\right\|_F^2 \leq C\sum_{K\in\mathcal{T}^\sharp}\left\|\mathfrak{p}^{-2}h_K\nabla p_h\right\|_K^2.
$$

Proceeding in a similar way for the other terms, we obtain (43).

Finally, we collect inequalities (40)–(42) and we choose $(\mathbf{v}_h, q_h) = (\mathbf{u}_h, -p_h) + \zeta_1(-\mathbf{w}_h, 0) + \zeta_2(-\mathfrak{p}^{-4}h_K^2\nabla p_h, 0)$. Then, we obtain that

$$
\begin{aligned}
&A_h(\mathbf{u}_h, p_h; \mathbf{v}_h, q_h) \\
&\geq c_a\left|\left|\left|\mathbf{u}_h\right|\right|\right|_{V^c}^2 + \zeta_1(-C_1\left|\left|\left|\mathbf{u}_h\right|\right|\right|_{V^c}^2 + C_2\left\|p_h\right\|_{\Omega^\sharp}^2 \\
&\quad - C_3\sum_{K\in\mathcal{T}^\sharp}\left\|\mathfrak{p}^{-2}h_K\nabla p_h\right\|_K^2 - C_3\sum_{F\in\mathcal{F}_{int}^\sharp}\left\|\mathfrak{p}^{-1}h_F{}^{1/2}[\![p_h]\!]\right\|_F^2) \\
&\quad + \zeta_2(-C_4\left|\left|\left|\mathbf{u}_h\right|\right|\right|_{V^c}^2 + C_5\sum_{K\in\mathcal{T}^\sharp}\left\|\mathfrak{p}^{-2}h_K\nabla p_h\right\|_K^2 + C_6\sum_{F\in\mathcal{F}_{int}^\sharp}\left\|\mathfrak{p}^{-1}h_F^{1/2}[\![p_h]\!]\right\|_F^2) \\
&\geq (c_a - \zeta_1C_1 - \zeta_2C_4)\left|\left|\left|\mathbf{u}_h\right|\right|\right|_{V^c}^2 + \zeta_1C_2\left\|p_h\right\|_{\Omega^\sharp}^2 + (\zeta_2C_5 - \zeta_1C_3)\sum_{K\in\mathcal{T}^\sharp}\left\|\mathfrak{p}^{-2}h_K\nabla p_h\right\|_K^2 \\
&\quad + (\zeta_2C_6 - \zeta_1C_3)\sum_{F\in\mathcal{F}_{int}^\sharp}\left\|\mathfrak{p}^{-1}h_F^{1/2}[\![p_h]\!]\right\|_F^2.
\end{aligned}
\tag{44}
$$

We force $\zeta_1 \leq C_3^{-1}\min\{C_5, C_6\}\zeta_2$ or $\zeta_2 \geq C_3\min\{C_5C_6\}^{-1}\zeta_1$ and we choose $\zeta_2 = 2C_3\min\{C_5C_6\}^{-1}\zeta_1$. We finally impose $\zeta_1 \leq c_a/(C_1 + 2C_3\min\{C_5, C_6\}^{-1})$ and we conclude that

$$
A_h(\mathbf{u}_h, p_h; \mathbf{v}_h, q_h) \leq C(\left|\left|\left|\mathbf{u}_h\right|\right|\right|_{V^c}^2 + \left|\left|\left|p_h\right|\right|\right|_{Q^c}^2) = C\left|\left|\left|(\mathbf{u}_h, p_h)\right|\right|\right|_{V^c,Q^c}^2, \text{ for } C > 0.
$$

We now note that

$$\begin{aligned}
&\left|\!\left|\!\left|(\mathbf{u}_h-\zeta_1\mathbf{w}_h-\zeta_2\mathfrak{p}^{-4}h_K^2\nabla p_h,-p_h)\right|\!\right|\!\right|^2_{V^c,Q^c}\\
=&\left|\!\left|\!\left|\mathbf{u}_h-\zeta_1\mathbf{w}_h-\zeta_2\mathfrak{p}^{-4}h_K^2\nabla p_h\right|\!\right|\!\right|^2_{V^c}+|\!|\!|p_h|\!|\!|^2_{Q^c}\\
\leq&|\!|\!|\mathbf{u}_h|\!|\!|^2_{V^c}+\zeta_1|\!|\!|\mathbf{w}_h|\!|\!|^2_{V^c}+\zeta_2\left|\!\left|\!\left|\mathfrak{p}^{-4}h_K^2\nabla p_h\right|\!\right|\!\right|^2_{V^c}+|\!|\!|p_h|\!|\!|^2_{Q^c}\\
\leq&|\!|\!|\mathbf{u}_h|\!|\!|^2_{V^c}+(\zeta_1+2CC_3\min\{C_5,C_6\}^{-1}\zeta_1+1)|\!|\!|p_h|\!|\!|^2_{Q^c}\\
\leq&\big((\zeta_1(1+2CC_3\min\{C_5,C_6\}^{-1}))+1\big)|\!|\!|(\mathbf{u}_h,p_h)|\!|\!|^2_{V^c,Q^c},
\end{aligned}$$

and the proof of (39) follows, where $c_{bil}=\frac{\min\{c_a-\zeta_1(C_1+2C_3\min\{C_5C_6\}^{-1})C_4,\zeta_1C_2\}}{\zeta_1(1+C2C_3\min\{C_5,C_6\}^{-1})+1}$. □

5. Error estimates

Estimating the inconsistency of the bilinear form by the best approximation estimates, we have the following approximate Galerkin orthogonality. To obtain error estimates, in this section we will assume that the exact solution $(\mathbf{u},p)\in\left[H_0^1(\Omega^\sharp)\right]^d\times L_0^2(\Omega^\sharp)$.

Lemma 5.1. *Let* $(\mathbf{u},p)\in\left[H^2(\Omega^\sharp)\cap H_0^1(\Omega^\sharp)\right]^d\times\left[H^1(\Omega^\sharp)\cap L_0^2(\Omega^\sharp)\right]$ *be the solution to the Stokes problem* (1) *and* $(\mathbf{u}_h,p_h)\in V_h^\sharp\times Q_h^\sharp$ *the finite element approximation in* (6), with $h=\max_{\mathcal{K}\in\mathcal{T}^{cov}}h_{\mathcal{K}}$ due to shape regularity of $\mathcal{T}^{cov}$, see also Assumption 3.8. *Then,*

$$A_h(\mathbf{u}-\mathbf{u}_h,p-p_h;\mathbf{v}_h,q_h)=\mathcal{O}(h^{\mathfrak{p}}/\mathfrak{p}^{\mathfrak{p}-\frac{1}{2}})\quad\text{for every}\quad(\mathbf{v}_h,q_h)\in V_h^\sharp\times Q_h^\sharp. \tag{45}$$

Next, we prove the a priori error estimate and optimal convergence rates for the velocity and pressure.

Theorem 5.2. *Let* $(\mathbf{u},p)\in\left[H^{\mathfrak{p}+1}(\Omega^\sharp)\cap H_0^1(\Omega^\sharp)\right]^d\times\left[H^{\mathfrak{p}}(\Omega^\sharp)\cap L_0^2(\Omega^\sharp)\right]$ *be the solution to the Stokes problem* (1) *and* $(\mathbf{u}_h,p_h)\in V_h^\sharp\times Q_h^\sharp$ *the finite element approximation in agreement with* (6). *Then, there exists a constant* $C>0$, *such that*

$$|\!|\!|(\mathbf{u}-\mathbf{u}_h,p-p_h)|\!|\!|\leq C\sum_{K\in\mathcal{T}^\sharp}\frac{h_K^{\mathfrak{p}}}{\mathfrak{p}^{\mathfrak{p}-\frac{1}{2}}}\Big(||\mathbf{u}||_{\mathfrak{p}+1,K}+\frac{1}{\mathfrak{p}^{\frac{1}{2}}}||p||_{\mathfrak{p},K}\Big). \tag{46}$$

Proof. We start by rearranging the $(\mathbf{u}-\mathbf{u}_h,p-p_h)$ error adding and subtracting appropriate terms, and we conclude to its discrete and projection error components:

$$|\!|\!|(\mathbf{u}-\mathbf{u}_h,p-p_h)|\!|\!|\leq|\!|\!|(\mathbf{u}-\boldsymbol{\pi}_{\mathfrak{p}}\mathbf{u},p-\pi_{\mathfrak{p}}p)|\!|\!|+|\!|\!|(\boldsymbol{\pi}_{\mathfrak{p}}\mathbf{u}-\mathbf{u}_h,\pi_{\mathfrak{p}}p-p_h)|\!|\!|.$$

The first term optimal estimate is provided by (28) and (29) as it is proven in Corollary 4.4. The second term first is bounded by

$$|\!|\!|(\boldsymbol{\pi}_{\mathfrak{p}}\mathbf{u}-\mathbf{u}_h,\pi_{\mathfrak{p}}p-p_h)|\!|\!|\leq C|\!|\!|(\boldsymbol{\pi}_{\mathfrak{p}}\mathbf{u}-\mathbf{u}_h,\pi_{\mathfrak{p}}p-p_h)|\!|\!|_{V^c,Q^c},$$

according to (9). Due to (45) from Lemma 5.1 and Theorem, 4.7 there exists a pair $(\mathbf{v}_h,q_h)\in V_h^\sharp\times Q_h^\sharp$ with $\|(\mathbf{v}_h,q_h)\|_{V^c,Q^c}=1$, such that

$$\begin{aligned}
c_{bil}|\!|\!|(\boldsymbol{\pi}_{\mathfrak{p}}\mathbf{u}-\mathbf{u}_h,\pi_{\mathfrak{p}}p-p_h)|\!|\!|_{V^c,Q^c}\leq&A_h(\boldsymbol{\pi}_{\mathfrak{p}}\mathbf{u}-\mathbf{u}_h,\pi_{\mathfrak{p}}p-p_h;\mathbf{v}_h,q_h)\\
=&A_h(\boldsymbol{\pi}_{\mathfrak{p}}\mathbf{u}-\mathbf{u},\pi_{\mathfrak{p}}p-p;\mathbf{v}_h,q_h).
\end{aligned}$$

Hence, we use the definition of the corresponding form A_h to take

$$\begin{aligned}
&A_h(\boldsymbol{\pi}_{\mathfrak{p}}\mathbf{u}-\mathbf{u},\pi_{\mathfrak{p}}p-p;\mathbf{v}_h,q_h)\\
=&\widetilde{a}_h(\boldsymbol{\pi}_{\mathfrak{p}}\mathbf{u}-\mathbf{u},\mathbf{v}_h)+b_h(\mathbf{v}_h,\pi_{\mathfrak{p}}p-p)+b_h(\boldsymbol{\pi}_{\mathfrak{p}}\mathbf{u}-\mathbf{u},q_h).
\end{aligned} \tag{47}$$

Next, recalling that the pair $(\mathbf{v}_h, q_h)$ has unit $|||\cdot|||_{V^c,Q^c}$ norm, we derive

$$A_h(\boldsymbol{\pi}_{\mathfrak{p}}\mathbf{u}-\mathbf{u}, \pi_{\mathfrak{p}}p-p; \mathbf{v}_h, q_h) \leq C_a|||\boldsymbol{\pi}_{\mathfrak{p}}\mathbf{u}-\mathbf{u}||| \cdot |||v_h||| + C_b|||v_h||| \cdot |||\pi_{\mathfrak{p}}p-p_h||| + C_b|||\boldsymbol{\pi}_{\mathfrak{p}}\mathbf{u}-\mathbf{u}||| \cdot |||q_h|||,$$

and after employing the continuity of $\widetilde{a}_h$ and b_h in (20)–(22) and Corollary 4.4, also bounds the remaining terms. At this end, an estimate for (47) follows as

$$\begin{aligned} &A_h(\boldsymbol{\pi}_{\mathfrak{p}}\mathbf{u}-\mathbf{u}, \pi_{\mathfrak{p}}p-p; \mathbf{v}_h, q_h) \\ \leq& C \sum_{K\in\mathcal{T}^\sharp} \frac{h_K^{\mathfrak{p}}}{\mathfrak{p}^{\mathfrak{p}-\frac{1}{2}}} \left\{ \max\{|||v_h||| \cdot |||q_h|||\} \left(3||\mathbf{u}||_{\mathfrak{p}+1,K} + \frac{1}{\mathfrak{p}^{\frac{1}{2}}}||p||_{\mathfrak{p},K} \right) \right\} \\ \leq& C \sum_{K\in\mathcal{T}^\sharp} \frac{h_K^{\mathfrak{p}}}{\mathfrak{p}^{\mathfrak{p}-\frac{1}{2}}} \Big(||\mathbf{u}||_{\mathfrak{p}+1,K} + \frac{1}{\mathfrak{p}^{\frac{1}{2}}}||p||_{\mathfrak{p},K} \Big), \end{aligned}$$

and the estimate (46) follows. It is also necessary to check that the extended bilinear form $\tilde{a}_h(\cdot,\cdot)$ and the related inconsistency error bound does not affect the aforementioned optimal error bound, see also [14, Section 4.2]. This can easily be verified by employing again the tools of Corollary 4.4. In particular, we consider the residual $R_h(\boldsymbol{v_h}) := \tilde{a}_h(\boldsymbol{u}, \boldsymbol{v_h}) - a_h(\boldsymbol{u}, \boldsymbol{v_h})$, we substitute the bilinear forms with their components as in Subsection 2.2, we recall that $\boldsymbol{u}$ belongs in $V^\sharp$, e.g. $[\![\mathbf{u}]\!]$ is zero, on the boundary $\boldsymbol{u}|_\Gamma = 0$, and the residual becomes

$$-\sum_{F\in\mathcal{F}^\sharp_{int}\cup\Gamma} \int_F \left(\{\!\{ \boldsymbol{\Pi}_{\mathbf{L^2}}(\nabla\mathbf{u}) - \nabla\mathbf{u} \}\!\} \cdot \mathbf{n_F} [\![\mathbf{v_h}]\!] \right) d\gamma - \int_\Gamma \left(\mathbf{v}_h \boldsymbol{\Pi}_{\mathbf{L^2}}(\nabla\mathbf{u}) - \nabla\mathbf{u} \right) \cdot \mathbf{n}_\Gamma \big) \, d\gamma,$$

or

$$\begin{aligned} |R_h(\boldsymbol{v_h})| \leq& \sum_{F\in\mathcal{F}^\sharp_{int}\cup\Gamma} \int_F |\{\!\{ \boldsymbol{\Pi}_{\mathbf{L^2}}(\nabla\mathbf{u}) - \nabla\mathbf{u} \}\!\} \cdot \mathbf{n_F} [\![\mathbf{v_h}]\!]| \, d\gamma \\ &+ \int_\Gamma \left| \mathbf{v}_h \boldsymbol{\Pi}_{\mathbf{L^2}}(\nabla\mathbf{u}) - \nabla\mathbf{u} \right) \cdot \mathbf{n}_\Gamma \big| \, d\gamma. \end{aligned}$$

Next, we add and subtract the term $\boldsymbol{\pi}_{\mathfrak{p}}\nabla\mathbf{u}$, and after algebraic calculations we derive that

$$\begin{aligned} &|R_h(\boldsymbol{v_h})| \\ \leq& \sum_{F\in\mathcal{F}^\sharp_{int}\cup\Gamma} \int_F |(\{\!\{ \nabla\mathbf{u} - \boldsymbol{\pi}_{\mathfrak{p}}\nabla\mathbf{u} \}\!\} \cdot \mathbf{n_F} [\![\mathbf{v_h}]\!]| + |\{\!\{ \boldsymbol{\Pi}_{\mathbf{L^2}}(\nabla\mathbf{u}) - \boldsymbol{\pi}_{\mathfrak{p}}\nabla\mathbf{u} \}\!\} \cdot \mathbf{n_F} [\![\mathbf{v_h}]\!]|) \, d\gamma \\ &+ \int_\Gamma \mathbf{v}_h \big(|\nabla\mathbf{u} - \boldsymbol{\pi}_{\mathfrak{p}}\nabla\mathbf{u}| + |\boldsymbol{\Pi}_{\mathbf{L^2}}(\nabla\mathbf{u}) - \boldsymbol{\pi}_{\mathfrak{p}}\nabla\mathbf{u}| \big) \cdot \mathbf{n}_\Gamma \, d\gamma \\ \leq& \sum_{F\in\mathcal{F}^\sharp_{int}\cup\Gamma} \int_F |(\{\!\{ \nabla\mathbf{u} - \boldsymbol{\pi}_{\mathfrak{p}}\nabla\mathbf{u} \}\!\} \cdot \mathbf{n_F} [\![\mathbf{v_h}]\!]| + |\{\!\{ \boldsymbol{\Pi}_{\mathbf{L^2}}(\nabla\mathbf{u} - \boldsymbol{\pi}_{\mathfrak{p}}\nabla\mathbf{u}) \}\!\} \cdot \mathbf{n_F} [\![\mathbf{v_h}]\!]|) \, d\gamma \\ &+ \int_\Gamma \mathbf{v}_h \big(|\nabla\mathbf{u} - \boldsymbol{\pi}_{\mathfrak{p}}\nabla\mathbf{u}| + |\boldsymbol{\Pi}_{\mathbf{L^2}}(\nabla\mathbf{u} - \boldsymbol{\pi}_{\mathfrak{p}}\nabla\mathbf{u})| \big) \cdot \mathbf{n}_\Gamma \, d\gamma. \end{aligned}$$

Finally, for the last inequality terms we use the fact that $\boldsymbol{\Pi}_{\mathbf{L^2}}\boldsymbol{\pi}_{\mathfrak{p}}\mathbf{v}$ coincides with $\boldsymbol{\pi}_{\mathfrak{p}}\mathbf{v}$, we follow the same procedure as in the beginning of the present proof, the tools as demonstrated in Collorary 4.4, that the projector $\boldsymbol{\Pi}_{\mathbf{L^2}}$ has the stability property $||\boldsymbol{\Pi}_{\mathbf{L^2}}\mathbf{v}||_{L^2(K)} \leq ||\mathbf{v}||_{L^2(K)}$, and we verify that the related inconsistency error bound does not affect the aforementioned optimal error bound. □

Remark 5.3. We note that if one makes stronger assumptions as mesh quasi-uniformity: $h = \max_{K\in\mathcal{T}^\sharp} h_K$, then the estimate of Theorem 5.2 is transformed to $|||(\mathbf{u}-\mathbf{u}_h, p-p_h)|||\leq C\frac{h^{\mathfrak{p}}}{\mathfrak{p}^{\mathfrak{p}-\frac{1}{2}}}\Big(||\mathbf{u}||_{\mathfrak{p}+1,\Omega^\sharp} + \frac{1}{\mathfrak{p}^{\frac{1}{2}}}||p||_{\mathfrak{p},\Omega^\sharp}\Big)$, which verifies optimal convergence in h and suboptimal in p by $p^{1/2}$.

6. Numerical Experiments/Convergence tests

6.1. 1st experiment: Rectangular domain $\Omega^\sharp$. We consider a two–dimensional test case of (1) in the unit square $\Omega^\sharp = [0,1]^2$ with exact solution

$$\mathbf{u}(x,y) = (u(x,y), -u(y,x)), \quad p(x,y) = \sin(2\pi x)\cos(2\pi y),$$

where $u(x,y) = (\cos(2\pi x) - 1)\sin(2\pi y)$.

Note that the mean value of $p(x,y)$ over $\Omega^\sharp$ vanishes by construction, thus ensuring that the problem (1) is uniquely solvable. As in subsection 2.2, in the spirit of arbitrarily shaped discontinuous Galerkin method on the boundary approach, we consider the original domain $\Omega^\sharp$ as seen in Figure 1's first geometry. A level set description of the geometry is possible through the function

$$\phi(x,y) = |x-0.5| + |y-0.5| + ||x-0.5| - |y-0.5|| - 1 < 0. \tag{48}$$

To investigate the error convergence behavior of the discretization (6), we consider a sequence of successively refined tessellations $\{\mathcal{T}^\sharp_{h_i}\}_{i>0}$ of $\Omega^\sharp$ with mesh parameters $h_i = 2^{-i-2}$, for $i = 0,\ldots,7$. As it is shown in the rectangular geometry case of Figure 2 exploiting the level-set function information on $\partial\Omega^\sharp$, elements containing straight faces approximating the polytopal boundary are marked. Finally, all marked elements are treated as classical triangular elements in the interior, with polytopal elements only on the boundary described by the domain level-set function, thus capturing the domain exactly. To allow for several polynomial degrees $\mathfrak{p}_i$, the symmetric interior penalty parameter in (4) scales as $\sigma = \mathfrak{p}_i^2/h_i$. A sparse solver has been used to solve the arising linear systems.

As expected from the theoretical error estimate stated in Theorem 5.2, optimal $\mathfrak{p}$-th order convergence rates with respect to the H^1–norm of the velocity error and the L^2–norm of the pressure error are in agreement with the error results as they are visualized in Table 1 ($\mathfrak{p}_1/\mathfrak{p}_0$) and Table 2 ($\mathfrak{p}_2/\mathfrak{p}_1$). Although, as seen in Table 3 ($\mathfrak{p}_3/\mathfrak{p}_2$) the convergence rates are optimal for the velocity and suboptimal for pressure. The superiority of the higher order framework is obvious and show that the method is efficient. Numerical experiments verify these facts, indeed, for larger $\mathfrak{p}$, much smaller errors are attained in progressively coarser meshes, for $\mathfrak{p}_i/\mathfrak{p}_{i-1}$ Taylor–Hood velocity/pressure pairs order, and the inf–sup stability is guaranteed. The aforementioned results are visualized in Figure 4.

Moreover in Table 4, and in the context of [2], a sequence of $\mathfrak{p}_3/\mathfrak{p}_2$ approximations for the velocity and pressure solution in progressively finer meshes is illustrated, showcasing the convergence of the method and the errors with respect to several mesh sizes. Further investigation, revealed that contrasting the results between Table 3 and Table 4 related to the $\mathfrak{p}_3/\mathfrak{p}_2$ case, i.e. comparing the suggested in the present work framework without any ghost type of stabilization on the boundary zone area, against to the full ghost penalty stabilization, showed that: the suggested method, yields better error behavior and better convergence rates only for the velocity, although suboptimal for the pressure even if the errors are better, a phenomenon that will be discussed later and it is probably caused by the quadrature on the polytopal boundary elements we employed. Therefore, we

TABLE 1. Rectangular geometry: Errors and rates of convergence with respect to H^1-norm for the velocity and L^2-norm for the pressure, using $\mathfrak{p}_1/\mathfrak{p}_0$ finite elements.

Discretization	Errors and convergence rates: $\mathfrak{p}_1/\mathfrak{p}_0$ polynomials case			
$h_{\max}$	$\|\mathbf{u}-\mathbf{u}_h\|_{1,\Omega^\sharp}$	Conv. rate	$\|p-p_h\|_{\Omega^\sharp}$	Conv. rate
$0.25(=2^{-2})$	1.469461	–	0.8756151	–
$0.125(=2^{-3})$	0.871741	0.7533148	0.4336638	1.0137197
$0.0625(=2^{-4})$	0.526300	0.7280155	0.3289021	0.3989189
$0.03125(=2^{-5})$	0.290011	0.8597764	0.1901614	0.7904334
$0.015625(=2^{-6})$	0.151577	0.9360504	0.1006410	0.9180059
$0.0078125(=2^{-7})$	0.077476	0.9682347	0.0515098	0.9662987
$0.00390625(=2^{-8})$	0.039269	0.9803399	0.0261353	0.9788479
Mean:	–	0.8709553	–	0.8443707

TABLE 2. Rectangular geometry: Errors and rates of convergence with respect to H^1-norm for the velocity and L^2-norm for the pressure, using $\mathfrak{p}_2/\mathfrak{p}_1$ and finite elements.

Discretization	Errors and convergence rates: $\mathfrak{p}_2/\mathfrak{p}_1$ polynomials case			
$h_{\max}$	$\|\mathbf{u}-\mathbf{u}_h\|_{1,\Omega^\sharp}$	Conv. rate	$\|p-p_h\|_{\Omega^\sharp}$	Conv. rate
$0.25(=2^{-2})$	0.2372591	–	0.1131108	–
$0.125(=2^{-3})$	0.1129321	1.0710074	0.0512201	1.1429531
$0.0625(=2^{-4})$	0.0337229	1.7436526	0.0165609	1.6289302
$0.03125(=2^{-5})$	0.0088867	1.9240082	0.0046825	1.8224281
$0.015625(=2^{-6})$	0.0023107	1.9433135	0.0012434	1.9129403
$0.0078125(=2^{-7})$	0.0005816	1.9900301	0.0003073	2.0165782
Mean:	–	1.7344024	–	1.7047660

TABLE 3. Rectangular geometry: Errors and rates of convergence with respect to H^1-norm for the velocity and L^2-norm for the pressure, using $\mathfrak{p}_3/\mathfrak{p}_2$ finite elements.

Discretization	Errors and convergence rates: $\mathfrak{p}_3/\mathfrak{p}_2$ polynomials case			
$h_{\max}$	$\|\mathbf{u}-\mathbf{u}_h\|_{1,\Omega^\sharp}$	Conv. rate	$\|p-p_h\|_{\Omega^\sharp}$	Conv. rate
$0.25(=2^{-2})$	0.0466716	–	0.0184400	–
$0.125(=2^{-3})$	0.0076981	2.5999546	0.0069364	1.4105717
$0.0625(=2^{-4})$	0.0012099	2.6696092	0.0017273	2.0056609
$0.03125(=2^{-5})$	0.0001644	2.8789030	0.0009789	0.8192784
$0.015625(=2^{-6})$	2.5518e-05	2.6883086	0.0003071	1.6720465
Mean:	–	2.7091938	–	1.4768894

may avoid integration errors related to the normal derivative up to the third-order jump terms used in the ghost penalty stabilization approach, [42, 43], which lead to a significant improvement for the velocity and pressure errors, as well as, crucial

TABLE 4. Rectangular geometry: Errors and rates of convergence with respect to H^1-norm for the velocity and L^2-norm for the pressure, using $\mathfrak{p}_3/\mathfrak{p}_2$ finite elements with higher order ghost boundary elements area stabilization in the context of [2].

Discretization	Errors and convergence rates: $\mathfrak{p}_3/\mathfrak{p}_2$ polynomials case			
$h_{\max}$	$\|\mathbf{u}-\mathbf{u}_h\|_{1,\Omega^\sharp}$	Conv. rate	$\|p-p_h\|_{\Omega^\sharp}$	Conv. rate
$0.25(=2^{-2})$	0.3386166	–	0.7184173	–
$0.125(=2^{-3})$	0.0247465	3.7743523	0.0590158	3.60564722
$0.0625(=2^{-4})$	0.0039329	2.6535468	0.0096287	2.61568216
$0.03125(=2^{-5})$	0.0006434	2.6117326	0.0017089	2.4942619
$0.015625(=2^{-6})$	0.0002045	1.6536038	0.0003671	2.2187371
Mean:	–	2.67330889	–	2.73358212

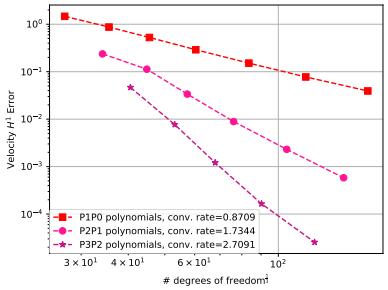

(a) $\|\mathbf{u}-\mathbf{u}_h\|_{1,\Omega^\sharp}$ error, conv.rates, and mean conv. rates

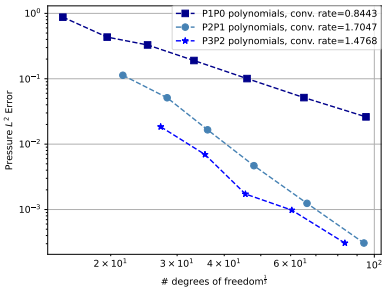

(b) $\|p-p_h\|_{\Omega^\sharp}$ error, conv.rates, and mean conv. rates

FIGURE 4. Rectangular geometry: Visualization of the H^1-norm velocity errors and L^2-norm pressure errors with respect to the discretization size.

computational cost savings. We again underline that the evaluation of boundary elements stabilization is avoided, namely, computations of gradually higher order normal derivative jumps –depended on the finite element order– seem unnecessary with the suggested approach. We also re-note that the pressure convergence rate in Table 3 is suboptimal although the error is much smaller e.g. than the case where full boundary area elements stabilization is applied for $\mathfrak{p}_3/\mathfrak{p}_2$ and as it is reported in Table 4. Finally, we report that in practice, the condition number for arbitrarily shaped boundary elements discontinuous Galerkin methods to solve Stokes problem is typically very large. The employment of efficient multigrid preconditioners for such cases, is left as a further challenge, see also the works [1], [20]. We also clarify that for the polytopal boundary elements, the current implementation performs quadrature by a sufficiently fine sub-triangulation approximating properly the curved element. Although, this first implementation of ours could be the issue of noticing slightly lower convergence rate than the predicted and specially on highest order polynomial case, and even worse for the pressure component. It is noted that in this case the sub-triangulation is only used to generate the quadrature rules. Of course, this is not the only possibility. For instance, domain-exact quadrature

algorithms for many curved domains exist, for such algorithms see [3, 21] and the references therein, and we plan to investigate this issue in the future.

6.2. 2nd experiment: Circular domain $\Omega^\sharp$. We consider a two–dimensional test case of (1) in $\Omega^\sharp$ to be a disc of radius $r = 1$ with exact solution

$$\mathbf{u}(x,y) = (u_x(x,y), u_y(y,x)),\ p(x,y) = (y^2+x^2-r^2)^2(2y^2+x^2)exp(-k(y^2+x^2))/2,$$

where

$$u_x = -y(y^2+x^2-r^2)exp(-k(y^2+x^2)/2) \text{ and } u_y = x(y^2+x^2-r^2)exp(-k(y^2+x^2)/2),$$

$k = 3\pi/2$. Note that the mean value of $p(x,y)$ over $\Omega^\sharp$ vanishes by construction, thus ensuring that the problem (1) is uniquely solvable as well as it is divergence free. Again, following subsection 2.2, in the spirit of arbitrarily shaped discontinuous Galerkin method on the boundary approach, we consider the original domain $\Omega^\sharp$ as it is in Figure 1's second image. A level set description of the geometry is possible through the function

$$\phi(x,y) = y^2 + x^2 - r^2 < 0. \tag{49}$$

We can easily confirm the results of Theorem 5.2 with the results as reported

TABLE 5. Circular geometry: Errors and rates of convergence with respect to H^1-norm for the velocity and L^2-norm for the pressure, using $\mathfrak{p}_1/\mathfrak{p}_0$ finite elements and with no ghost boundary elements area stabilization.

Discretization	Errors and convergence rates: $\mathfrak{p}_1/\mathfrak{p}_0$ polynomials case			
$h_{\max}$	$\|\mathbf{u}-\mathbf{u}_h\|_{1,\Omega^\sharp}$	Conv. rate	$\|p-p_h\|_{\Omega^\sharp}$	Conv. rate
0.62500625	0.2091145	–	0.1462374	–
0.31250312	0.1643200	0.3477844	0.0742179	0.9784737
0.15625156	0.0842741	0.9633462	0.0469684	0.6600764
0.07812578	0.0441366	0.9331140	0.0265372	0.8236700
0.03906289	0.0226625	0.9616639	0.0141321	0.9090371
0.01953144	0.0114507	0.9848749	0.0072050	0.9718974
0.00976572	0.0057310	0.9985631	0.0035962	1.0025094
Mean:	–	0.968312	–	0.873438

in Tables 5, 6, 7 for $\mathfrak{p} = 1, 2, 3$ respectively and for Taylor-Hood $\mathbf{u}$, p pairs. The superiority of the higher order cases is clarified, with respect to the errors and to the convergence rates where we manage better results in a much coarser mesh. This can also be seen with a glance in the visualization of Figure 5.

Finally, we highlight that the convergence rates for both tests seems to stop in the denser meshes and especially in the highest order polynomials rectangular geometry cases even if we notice good error results. This in our opinion happens due to the aforementioned way of integration on the polytopal boundary elements and we will leave the correction for the future, and of course crucial role played the corner points since in this last experiment –with the smoother circular geometry– we noticed correction of the pressure suboptimal convergence rates.

TABLE 6. Circular geometry: Errors and rates of convergence with respect to H^1-norm for the velocity and L^2-norm for the pressure, using $\mathfrak{p}_2/\mathfrak{p}_1$ finite elements and with no ghost boundary elements area stabilization.

Discretization	Errors and convergence rates: $\mathfrak{p}_2/\mathfrak{p}_1$ polynomials case			
$h_{\max}$	$\|\mathbf{u}-\mathbf{u}_h\|_{1,\Omega^\sharp}$	Conv. rate	$\|p-p_h\|_{\Omega^\sharp}$	Conv. rate
0.62500625	0.0328117	–	0.0145547	–
0.31250312	0.0319032	0.0405088	0.0123406	0.2380803
0.15625156	0.0082061	1.9589227	0.0039063	1.6595269
0.07812578	0.0020995	1.9666160	0.0010171	1.9412207
0.03906289	0.0005342	1.9746348	0.0002690	1.9189042
0.01953144	0.0001331	2.0038963	6.759e-05	1.9927008
Mean:	–	1.976017	–	1.878088

TABLE 7. Circular geometry: Errors and rates of convergence with respect to H^1-norm for the velocity and L^2-norm for the pressure, using $\mathfrak{p}_3/\mathfrak{p}_2$ finite elements and with no ghost boundary elements area stabilization.

Discretization	Errors and convergence rates: $\mathfrak{p}_3/\mathfrak{p}_2$ polynomials case			
$h_{\max}$	$\|\mathbf{u}-\mathbf{u}_h\|_{1,\Omega^\sharp}$	Conv. rate	$\|p-p_h\|_{\Omega^\sharp}$	Conv. rate
0.62500625	0.0120753	–	0.0070916	–
0.31250312	0.0044922	1.4265409	0.0014351	2.3048990
0.15625156	0.0005162	3.1212517	0.0001907	2.9113670
0.07812578	6.4007e-05	3.0118057	2.7194e-05	2.8103814
0.03906289	8.3068e-06	2.9458756	5.3857e-06	2.3361018
Mean:	–	2.62636850	–	2.5906872

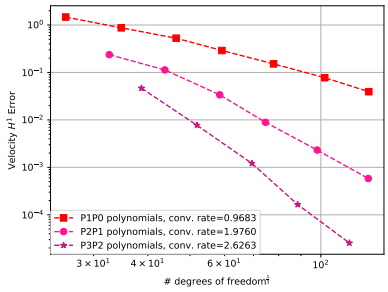

(a) $\|\mathbf{u}-\mathbf{u}_h\|_{1,\Omega^\sharp}$ error, conv.rates, and mean conv. rates

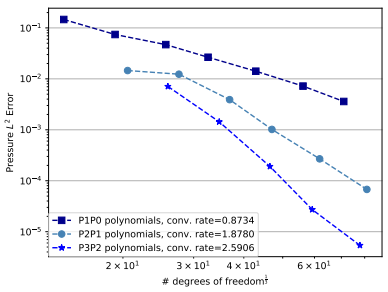

(b) $\|p-p_h\|_{\Omega^\sharp}$ error, conv.rates, and mean conv. rates

FIGURE 5. Circular geometry: Visualization of the H^1-norm velocity errors and L^2-norm pressure errors with respect to the discretization size.

7. Conclusion

In this effort, we proposed and tested a discontinuous Galerkin method for the incompressible Stokes flow employing arbitrarily shaped elements. *hp*-version optimal order convergence is proved for higher order finite elements of $\mathfrak{p}_i/\mathfrak{p}_{i-1}$ order for velocity and pressure fields. This method may prove valuable in applications where special emphasis is placed on the effective approximation of pressure, attaining much smaller errors in coarser meshes and whenever geometrical morphings are taking place. In fact, control over the error of the pressure field is among the most decisive points of difficulty for many methods. Numerical test experiments demonstrated the very good stability and accuracy properties of the method. The theoretical convergence rates for the H^1-norm of the velocity and the L^2-norm of the pressure have been validated by our tests, even for the $\mathfrak{p}_3/\mathfrak{p}_2$ case. Significantly smaller errors have been noticed considering the comparison of the method under consideration, with the unfitted dG finite element method of [2] and the results as reported in Table 3 and Table 4 for step $h = 2^{-6}$. In particular $2.5518e-05$, 0.0003071 for the presented approach, and 0.0002045, 0.0003671 for a fully stabilized with efficient ghost penalty fictitious domain FEM and for the velocity and pressure respectively have been reported. The latter, after comparison, shows smaller errors for the pressure and one order of magnitude better errors for the velocity which validates the superiority of the proposed approach. In the present work, we focused on the static Stokes problem. Thus, the method seems very promising. Future work will extend our investigations to more general fluid mechanics problems, including time-dependent problems on complex domains and/or nonlinearities, as well as, Navier-Stokes and fluid-structure interaction systems. Finally, future development would be a proper preconditioner and a reduced order modeling investigation.

Acknowledgments

This project has received funding from the "First Call for H.F.R.I. Research Projects to support Faculty members and Researchers and the procurement of high-cost research equipment" grant 3270 and was supported by computational time granted from the National Infrastructures for Research and Technology S.A. (GRNET S.A.) in the National HPC facility - ARIS - under project ID pa190902. The author would like also to thank Prof. Emmanuil Georgoulis from NTUA for valuable comments and inspiring ideas. We would like also to thank the contributors of the ngsolve-ngsxfem, [39, 51].

References

[1] A. Aretaki and E. N. Karatzas. Random geometries for optimal control PDE problems based on fictitious domain FEMs and cut elements. Journal of Computational and Applied Mathematics, 412:114286, 2022.

[2] A. Aretaki, E. N. Karatzas, and G. Katsouleas. Equal Higher Order Analysis of an Unfitted Discontinuous Galerkin Method for Stokes Flow Systems. J. Sci. Comput., 91(2):48, 2022.

[3] E. Artioli, A. Sommariva, and M. Vianello. Algebraic cubature on polygonal elements with a circular edge. Computers & Mathematics with Applications, 79(7):2057–2066, 2020. Advanced Computational methods for PDEs.

[4] A. Baker, W. N. Jureidini, and O. A. Karakashian. Piecewise solenoidal vector fields and the Stokes problem. SIAM J. Numer. Anal., 27:1466–1485, 1990.

[5] J. W. Barrett and C. M. Elliott. Fitted and Unfitted Finite-Element Methods for Elliptic Equations with Smooth Interfaces. IMA Journal of Numerical Analysis, 7(3):283–300, 07 1987.

[6] P. Bastian and C. Engwer. An unfitted finite element method using discontinuous Galerkin. J. Numer. Meth. Engrg., 79:1557–1576, 2009.

[7] P. Bastian, C. Engwer, J. Fahlke, and O. Ippisch. An unfitted discontinuous galerkin method for pore–scale simulations of solute transport. Math. Comput. Simulat., 81:2051–2061, 2011.
[8] L. Beirao Da Veiga, F. Brezzi, A. Cangiani, G. Manzini, L. D. Marini, and A. Russo. Basic principles of virtual element methods. Mathematical Models and Methods in Applied Sciences, 23(01):199–214, 2013.
[9] L. Beirao Da Veiga, K. Lipnikov, and G. Manzini. The mimetic finite difference method for elliptic problems. MS&A Modeling, Simulation and Applications Springer, Cham, 2014.
[10] W. Bo and J. W. Grove. volume of fluid method based ghost fluid method for compressible multi-fluid flows. Computers & Fluids, 90:113–122, 2014.
[11] E. Burman and P. Hansbo. Fictitious domain finite element methods using cut elements II. A stabilized Nitsche method, Appl. Num. Math., 62(4):328–341, 2012.
[12] E. Burman and P. Hansbo. Fictitious domain methods using cut elements: III. A stabilized Nitsche method for Stokes problem. ESAIM: Math. Model. Numer. Anal. 48(3), 859-874 (2014), 48(3):859–874, 2014.
[13] A. Cangiani, Z. Dong, and E. H. Georgoulis. hp-Version discontinuous Galerkin methods on essentially arbitrarily-shaped elements. Math. Comput., 91:1–35, 2022.
[14] A. Cangiani, Z. Dong, E.H. Georgoulis, and P. Houston. hp-Version Discontinuous Galerkin Methods on Polygonal and Polyhedral Meshes. SpringerBriefs in Mathematics. Springer International Publishing, 2017.
[15] B. Cockburn, J. Gopalakrishnan, and R. Lazarov. Unified Hybridization of Discontinuous Galerkin, Mixed, and Continuous Galerkin Methods for Second Order Elliptic Problems. SIAM Journal on Numerical Analysis, 47(2):1319–1365, 2009.
[16] B. Cockburn, G. Kanschat, D. Schötzau, and C. Schwab. Local discontinuous Galerkin methods for the Stokes system. SIAM J. Numer. Anal, 40:319–343, 2002.
[17] D. A. Di Pietro and A. Ern. Mathematical aspects of discontinuous Galerkin methods, volume 69. Springer, 2012.
[18] D. A. Di Pietro and A. Ern. A hybrid high-order locking-free method for linear elasticity on general meshes. Computer Methods in Applied Mechanics and Engineering, 283:1–21, 2015.
[19] H. Dong, B. Wang, Z. Xie, and L. Wang. An unfitted hybridizable discontinuous Galerkin method for the Poisson interface problem and its error analysis. IMA J. Numer. Anal., 37:444–476, 2016.
[20] Z. Dong. Discontinuous galerkin methods for the biharmonic problem on polygonal and polyhedral meshes. International Journal of Numerical Analysis and Modeling, Volume 16:825–846, 2019.
[21] Z. Dong, E. H. Georgoulis, and Kapas T. GPU-accelerated discontinuous Galerkin methods on polytopic meshes. SIAM J. Sci. Comput., 43:C312–C334, 2021.
[22] Z. Dong and L. Mascotto. *hp*-optimal interior penalty discontinuous Galerkin methods for the biharmonic problem. arXiv preprint arXiv:2212.03735, 2022.
[23] M. Duprez and A. Lozinski. ϕ–fem a finite element method on domains defined by level–sets. 2019. arXiv: 1901.03966v3.
[24] C. Engwer, S. May, A. Nüßing, and F. Streitbürger. A Stabilized DG Cut Cell Method for Discretizing the Linear Transport Equation. SIAM Journal on Scientific Computing, 42(6):A3677–A3703, 2020.
[25] C. Engwer, T. Ranner, and S. Westerheide. An unfitted discontinuous Galerkin scheme for conservation laws on evolving surfaces. Proceedings of the Conference Algoritmy, pages 44–54, 2016.
[26] T. Fries and T. Belytschko. The extended/generalized finite element method: An overview of the method and its applications. International Journal for Numerical Methods in Engineering, 84(3):253–304, 2010.
[27] E. H. Georgoulis, Edward J. C. Hall, and J. M. Melenk. On the Suboptimality of the p-Version Interior Penalty Discontinuous Galerkin Method. Journal of Scientific Computing, 42:54–67, 2010.
[28] V. Girault, B. Rivière, and M. A. Wheeler. Discontinuous Galerkin method with non–overlapping domain decomposition for the Stokes and Navier–Stokes problems. Math. Comput., 74:53–84, 2005.
[29] A. Hansbo and P. Hansbo. An unfitted finite element method, based on Nitsche's method, for elliptic interface problems. Comput. Methods Appl. Mech. Eng, 191:5537–5552, 2002.
[30] Paul Houston et al. Discontinuous hp-finite element methods for advection-diffusion-reaction problems. SIAM Journal on Numerical Analysis, 39(6):2133–2163, 2002.

[31] L. N. T. Huynh, N. C. Nguyen, J. Peraire, and B. C. Khoo. A high order hybrizidable discontinuous Galerkin method for elliptic interface problems. Int. J. Numer. Meth. Engrg., 93:183–200, 2013.
[32] E. N. Karatzas. Boundary and distributed optimal control for a population dynamics PDE model with discontinuous in time Galerkin FEM schemes. Comput. Math. Appl., 165(6):70–87, 2024.
[33] E. N. Karatzas, F. Ballarin, and G. Rozza. Projection-based reduced order models for a cut finite element method in parametrized domains. Computers & Mathematics with Applications, 3(79):833–851, 2020.
[34] E. N. Karatzas and G. Rozza. A Reduced Order Model for a Stable Embedded Boundary Parametrized Cahn-Hilliard Phase-Field System Based on Cut Finite Elements. J Sci Comput, 89(9):1–29, 2021.
[35] E. N. Karatzas, G. Stabile, N. Atallah, G. Scovazzi, and G. Rozza. A reduced order approach for the embedded shifted boundary fem and a heat exchange system on parametrized geometries. pages 22–25. IUTAM Symposium on Model Order Reduction of Coupled Systems, Stuttgart, Germany, May, 2018. IUTAM Bookseries, vol 36. Springer, Cham, 2020.
[36] E. N. Karatzas, G. Stabile, L. Nouveau, G. Scovazzi, and G. Rozza. A reduced basis approach for PDEs on parametrized geometries based on the shifted boundary finite element method and application to a Stokes flow. Comput. Methods Appl. Mech. Engrg., 347:568–587, 2019.
[37] E. N. Karatzas, G. Stabile, L. Nouveau, G. Scovazzi, and G. Rozza. A reduced-order shifted boundary method for parametrized incompressible Navier-Stokes equations. Comput. Methods Appl. Mech. Engrg., 370:113–273, 2020.
[38] E. M. Kolahdouz, A. P. S. Bhalla, B. A. Craven, and B. E. Griffith. An immersed interface method for faceted surfaces. Journal of Computational Physics, 400, 2020.
[39] C. Lehrenfeld, F. Heimann, J. Preuß , and H. von Wahl. ngsxfem: Add-on to ngsolve for geometrically unfitted finite element discretizations. Journal of Open Source Software, 6(64):32–37, 2021.
[40] A. Lozinski. Cutfem without cutting the mesh cells: a new way to impose dirichlet and neumann boundary conditions on unfitted meshes. Computer Methods in Applied Mechanics and Engineering, 356:75–100, 2019.
[41] A. Main and G. Scovazzi. The shifted boundary method for embedded domain computations. Part I: Poisson and Stokes problems. Journal of Computational Physics, 372:972–995, 2018.
[42] A. Massing, M. G. Larson, A. Logg, and M. E. Rognes. A stabilized Nitsche fictitious domain method for the Stokes problem. J. Sci. Comput., 61:604–628, 2014.
[43] A. Massing, M. G. Larson, A. Logg, and M. E. Rognes. A stabilized Nitsche overlapping mesh method for the Stokes problem. Numer. Math., 128:73–101, 2014.
[44] R. Massjung. An unfitted discontinuous galerkin method applied to elliptic interface problems. SIAM J. Numer. Anal., 50:3134–3162, 2012.
[45] J. M. Melenk. hp-finite element methods for singular perturbations. 2002.
[46] V. Murti and S. Valliappan. Numerical inverse isoparametric mapping in remeshing and nodal quantity contouring. Computers & Structures, 22(6):1011–1021, 1986.
[47] V. Murti, Y. Wang, and S. Valliappan. Numerical inverse isoparametric mapping in 3D FEM. Computers & Structures, 29(4):611–622, 1988.
[48] S. J. Osher and R. Fedkiw. Level set methods and dynamic implicit surfaces., volume 153 of Applied mathematical sciences. Springer, 2003.
[49] V. Pasquariello, F. Hammerl, G. Órley, S. Hickel, C. Danowski, A. Popp, W.A. Wall, and N.A. Adams. A cut-cell finite volume–finite element coupling approach for fluid–structure interaction in compressible flow. J. Comput. Phys., 307:670–695, 2016.
[50] C. S. Peskin. Flow patterns around heart valves: A numerical method. J. Comput. Phys., 10:252–271, 1972.
[51] J. Schberl, A. Arnold, J. Erb, J. M. Melenk, and T. P. Wihler. C++11 implementation of finite elements in NGSolve. Technical report, Institute for Analysis and Scientific Computing, Vienna University of Technology, 2014. ASC Report 30/2014.
[52] D. Schötzau, C. Schwab, and A. Toselli. Mixed hp-DGFEM for incompressible flows. SIAM J. Numer. Anal, 40:2171–2194, 2003.
[53] C. Schwab. *p*- and *hp*-Finite element methods: Theory and applications in solid and fluid mechanics. Oxford University Press: Numerical mathematics and scientific computation, 1998.
[54] N. Sukumar and A. Tabarraei. Conforming polygonal finite elements. International Journal for Numerical Methods in Engineering, 61(12):2045–2066, 2004.

[55] A. Toselli. *hp*-discontinuous Galerkin approximations for the Stokes problem. Mathematical Models and Methods in Applied Sciences, 12(11):1565–1597, 2002.
[56] Q. Wang and J. Chen. Unfitted discontinuous galerkin method for elliptic interface problems. Journal of Applied Mathematics, 13(3):1–10, 2014.
[57] C. H. Wu, O. M. Faltinsen, and B. F. Chen. Time-independent finite difference and ghost cell method to study sloshing liquid in 2d and 3d tanks with internal structures. Comm. Comput. Phys., 13(3):780–800, 2013.

School of Mathematics, Aristotle University of Thessaloniki, Thessaloniki 54124, Greece.
E-mail: ekaratza@math.auth.gr

SISSA, International School for Advanced Studies, Mathematics Area, mathLab, Trieste, Italy.
E-mail: ekaratza@sissa.it